AEDC-TR-70-102

Copy 1

SORPTION PUMPING OF HYDROGEN BY CRYODEPOSITS—DYNAMIC PUMPING CHARACTERISTICS

K. E. Tempelmeyer

ARO, Inc.

October 1970

VON KÁRMÁN GAS DYNAMICS FACILITY
ARNOLD ENGINEERING DEVELOPMENT CENTER
AIR FORCE SYSTEMS COMMAND
ARNOLD AIR FORCE STATION, TENNESSEE

NOTICES

When U. S. Government drawings specifications, or other data are used for any purpose other than a definitely related Government procurement operation, the Government thereby incurs no responsibility nor any obligation whatsoever, and the fact that the Government may have formulated, furnished, or in any way supplied the said drawings, specifications, or other data, is not to be regarded by implication or otherwise, or in any manner licensing the holder or any other person or corporation, or conveying any rights or permission to manufacture, use, or sell any patented invention that may in any way be related thereto.

Qualified users may obtain copies of this report from the Defense Documentation Center.

References to named commercial products in this report are not to be considered in any sense as an endorsement of the product by the United States Air Force or the Government.

SORPTION PUMPING OF HYDROGEN BY CRYODEPOSITS—DYNAMIC PUMPING CHARACTERISTICS

K. E. Tempelmeyer
ARO, Inc.

FOREWORD

The research presented in this report was sponsored by the Arnold Engineering Development Center (AEDC), Air Force Systems Command (AFSC), Arnold Air Force Station, Tennessee, under Program Element 61120F.

The results reported herein were obtained by ARO, Inc. (a subsidiary of Sverdrup & Parcel and Associates, Inc.), contract operator of AEDC, AFSC, under Contract F40600-71-C-0002. The research was conducted from April 1969 through September 1969, under ARO Project No. SW3003, and the manuscript was submitted for publication on March 13, 1970.

The work described herein is extracted from a larger effort which was submitted to satisfy the Ph.D. dissertation requirements for The University of Tennessee Space Institute (UTSI). The author would like to acknowledge many helpful suggestions, ideas, and comments, which contributed significantly to the progress of this work, from his colleagues, Mr. R. Dawbarn, Dr. Allie Smith, and Mr. Donald Todd, as well as from his thesis advisor, Dr. R. L. Young, Deputy Director for Educational Programs at UTSI.

This technical report has been reviewed and is approved.

Michael G. Buja
First Lieutenant, USAF
Research and Development Division
Directorate of Technology

Harry L. Maynard
Colonel, USAF
Director of Technology

ABSTRACT

The sorption for cryodeposited frosts for hydrogen has been investigated both analytically and experimentally. Most of the experimental tests were carried out with carbon dioxide frost at temperatures between 12 and 22°K as the cryosorbent and hydrogen at 300°K as the sorbate. Dynamic pumping characteristics of the sorbent-sorbate combination were systematically measured for chamber pressures between 10^{-7} and 10^{-4} torr. Additional experimental results were obtained with sulphur dioxide and methyl chloride cryosorbents. An initial hydrogen pumping speed of 30 liters/cm^2-sec was measured for 12°K carbon dioxide frost which was equivalent to an initial effective capture probability of about 0.7. The initial pumping speed appears to be governed by the sorbent, sorbate-surface interaction and may be increased somewhat by forming the surface in a manner to make it smoother but at the consequence of an attendant loss of sorption capacity. The pumping speed of a frost cryosorbent decreases with increasing amount of gas sorbed. A model of the sorption dynamics was formulated. An approximate closed-form solution was obtained in the limit of rather compact frosts whose sorption behavior would be limited by the ability of the molecules to penetrate and diffuse into the frost. Theoretical calculations for this limiting case agreed with the observed pumping characteristics of the more compact frosts. Consequently, it is believed that the formulation of the frost cryosorption theory is proper. Comparisons between theory and experiment indicated that the diffusion constant for hydrogen in a variety of cryodeposits varied from 10^{-8} to 10^{-15} cm^2/sec. Also, it was noted that carbon dioxide and sulphur dioxide frosts deposited at temperatures below 30°K appear to undergo some crystal transition if their temperature is increased to above 30°K.

CONTENTS

APPENDIXES

I. ILLUSTRATIONS

Figure

NOMENCLATURE

A	Area
$A_1, A_2, B_1, B_2, C_1, C_2$	Constants
C	Dimensionless sorption capacity, ratio of the number of molecules sorbed to the number of molecules predeposited in the frost sorbent
c	Sticking probability
D	Diffusion constant
E_B	Surface barrier energy

E_D	Diffusion energy
E_d	Desorption energy
G	Mass transfer constant
J	Molecular flux, molecules/cm^2-sec
J_o	Initial pumped flux
K	Leak conductance
k	Boltzmann constant
ℓ	Frost thickness
$\bar{\ell}$	Mean thickness of frost sorbent
m	Mass of a molecule
N	Number of sorbed molecules
N_D	Diffusion Biot number
N_F	Fourier modulus
N_o	Number of adsorbed molecules on surface
n	Number density of sorbed particles
$\dot{n}$	Molecular strike rate
n*	Calculated mean number of molecules sorbed/unit volume of frost
n′	Transformed number density, $n' = n-n_o$
n_o	Equilibrium number density at surface
n,m	Summation indices
P	Pressure
Q	Quantity of gas, torr-liters
$\dot{Q}$	Throughput, torr-liters/sec
r	Radial distance

S	Pumping speed
S_o	Initial pumping speed
s	Unit pumping speed
s_o	Initial unit pumping speed
T	Temperature
$T(t)$	A function only of time
t	Time
t_r	Residence time
V	Volume
$V(r)$	Potential energy as a function of r
$X(x)$	A function only of x
x	Coordinate
ϵ	Lennard-Jones well depth
$\lambda^{(n)}$	Characteristic value
ρ	Density
σ	Lennard-Jones well depth distance
τ	Period of vibration of adsorbed molecule
ψ	Functions defined by Eqs. (II-27) and (II-28)

SUBSCRIPTS

1	Region 1, thin surface layer
2	Region 2, bulk of frost
a	Gas addition system or adsorbed
add	Added
c	Chamber

d	Desorbed
f	Frost
form	Formation
g	Gas
i	Incident
j	Sorbate specie type
k	Sorbent specie type
liq	Liquid
max	Maximum
out	Outgassing
p	Pumped
r	Reflected
s	Sorbent in gas state
sat	Saturation
u	Ultimate

SECTION I
INTRODUCTION

Although cryopumping is widely used to produce low pressures in relatively large vacuum chambers, it is not often economically feasible for the removal of hydrogen, neon, and helium because of the low condensation temperatures of these gases at low pressures. Neon does not generally present a problem because of its rarity. However, hydrogen and helium are present in most vacuum systems and often limit the ultimate pressure which may be achieved. Moreover, these gases are widely used in aerospace technology, and frequently it is necessary to remove large amounts of them from space simulation chambers.

Recently, cryodeposited frosts formed by condensing certain gases (such as carbon dioxide, argon, oxygen, and nitrogen) on surfaces at temperatures between 10 and 20°K have been shown (Refs. 1 to 6) to provide an effective means to pump hydrogen by some adsorption-absorption process (Fig. 1, Appendix I). Moreover, these frosts will also effectively pump helium if the cryosurface temperature is maintained at 4.2°K and below (see Refs. 7 to 9). Because frost cryosorbents offer a number of advantages over other sorption pumping methods, this technique has been studied in some detail by the present author.

Sorption pumping is basically a dynamic process during which the pumping speed decreases from some initial value, and approaches zero as the frost is saturated by the sorbate at some equilibrium condition. There are two aspects of sorption: (1) the conditions for equilibrium and (2) the dynamics of sorption. The first has been considered in two previous reports (Refs. 10 and 11), which establish how much gas can be sorbed when equilibrium is attained. The second, which involves a description of how this equilibrium condition is achieved, is treated here.

The pumping process is first considered from a theoretical viewpoint, and a frost cryosorption theory is proposed. Experimental measurements of the hydrogen pumping speeds of several frost sorbents have been made and are compared to the theoretical calculations.

SECTION II
THEORY FOR FROST CRYOSORPTION

2.1 SORPTION PROCESS

When a gas molecule collides or interacts with a solid surface it may (1) reflect elastically; (2) reflect inelastically, in which case the energy exchange may be characterized by the energy accommodation coefficient; or (3) lose sufficient energy that it is physically adsorbed for at least a short time. If the particle is adsorbed, (1) it may remain on the surface for long times by condensation or chemisorption mechanisms, (2) it may be desorbed, or (3) it may diffuse over the surface or into the substrate material. The details of the gas-surface interaction are primarily governed by the interaction potential between the gas and surface material, the nature of the surface, and the gas and surface temperatures (Ref. 12).

2.1.1 Physical Adsorption

Because the physical character of the surfaces of frost cryosorbents is unknown and the interaction potential is extremely complex, one can form, at best, only an idealized qualitative picture of the sorbate-sorbent interaction, as sketched in Fig. 2a. For simplicity only the dimension normal to the surface is shown. A free molecule in the gas phase has some energy at point (a) and as it approaches the surface it experiences an attractive force. If in the interaction the molecule gives up some of its energy to the surface, it may not have sufficient energy to escape from the potential well. Once caught at some energy level in the well, say point (b), the molecule may undergo a relaxation process and attain thermal equilibrium with the solid (see Ref. 12). If the solid is cooled this would result in the molecule residing near the bottom of the well [point (c)]. At this point it is physically adsorbed. It will remain adsorbed in the potential well until it receives enough energy from the surface or from other incident molecules to escape. Frenkel (Ref. 13) has deduced from statistical considerations that on the average the particle will reside on the surface for the time,

$$t_r = \tau \exp (E_d/kT_f) \tag{1}$$

The residence time on the surface (t_r) can obviously be increased by decreasing the surface temperature. In this case the adsorbed molecules would reside near the bottom of the well with a smaller statistical chance of receiving enough energy from the surface to be desorbed. This is, of course, the basis of cryopumping. In this case the surface temperature is reduced to less than the vapor-pressure temperature (Ref. 14) so that adsorbed molecules have a very low probability of being desorbed and remain in a condensed, solidified form on the surface. Gas can be continuously pumped as long as the frost surface is maintained at or below the required temperature.

2.1.2 Cryosorption

The situation with cryosorption pumping is different. Experimental cryosorption test results of Refs. 10 and 11 show that physically adsorbed molecules are not bound to the surface but diffuse or migrate into the cryosorbent. This has the effect of removing the repulsive part of the interaction normally imposed by a solid surface and may be depicted by the gas-surface interaction potential distribution sketched in Fig. 2b.

The adsorbed molecule must overcome a potential barrier, E_B, in order to migrate away from its adsorption site and into the sorbent. This barrier must be considerably less than the depth of the adsorptive potential well, if sorption is to be much more probable than desorption. As a sorbed molecule diffuses further into the sorbent, it must overcome various diffusion potential barriers (E_D). These internal barriers may have heights different from those near the surface because the forces retarding diffusion away from the surface may be considerably different from those retarding diffusion within the porous structure of the sorbent. This occurs because the adsorbed molecule interacts with sorbent molecules in a two-dimensional sense on the surface, whereas a sorbed molecule will interact with sorbent molecules in three dimensions within small pores in the sorbent. For cryosorption pumping the surface temperature obviously need not be low

enough to cryopump the sorbate gas, but it must be low enough so that the adsorbed molecules have a low probability of being desorbed, thus giving them a better chance of being absorbed than being desorbed. In general, sorption pumping may be governed by one or some combination of the following factors: (1) the rate at which molecules are adsorbed on the surface, (2) the rate at which they enter the interior of the frost, and (3) their diffusion rate in the frost structure.

A simple analysis indicates how these various factors affect the pumping speed. The flux of molecules incident on the surface is

$$J_i = \frac{P}{\sqrt{2\pi m k T_g}} \tag{2}$$

and the flux at which some are directly reflected would be

$$J_r = (1 - c) \frac{P}{\sqrt{2\pi m k T_g}} \tag{3}$$

As a result, the molecular flux adsorbed by any surface is the product of the strike rate and the sticking probability,

$$J_a = J_i - J_r = \frac{cP}{\sqrt{2\pi m k T_g}} \tag{4}$$

In addition, adsorbed molecules may be desorbed, and the flux of desorbed particles is equal to the number of molecules per unit area on the surface divided by their mean residence time [Eq. (1)], or

$$J_d = \frac{N_o}{A_f t_r} = \frac{N_o}{A_f \tau} e^{-E_d/kT_f} \tag{5}$$

Consequently, the net flux of pumped molecules is the difference between Eqs. (4) and (5), or

$$J_p = \frac{c\,P}{\sqrt{2\pi m k T_g}} - \frac{N_o}{A_f \tau} e^{-E_d/kT_f} \tag{6}$$

Equation (6) was obtained from a balance of molecules to and from the surface. In addition, the flux of pumped molecules is also equal to the rate at which they might accumulate on the surface plus the rate at which they might diffuse into the frost, which may be written

$$J_p = \frac{1}{A_f} \frac{\partial N(\ell, t)}{\partial t} - D \frac{\partial n(\ell', t)}{\partial x} \tag{7}$$

where ℓ denotes the frost surface and ℓ' a position just inside the frost. The first term on the right-hand side accounts for the possibility of storage of adsorbed molecules on the

surface and the second for diffusion of molecules into the frost. Thus, the condition at the frost surface would be obtained by equating Eqs. (6) and (7),

$$\frac{c\,P}{\sqrt{2\pi m k\,T_g}} - \frac{N(\ell,t)}{A_f\,\tau} e^{-E_d/kt_f} = \frac{1}{A_t}\frac{\partial N(\ell,t)}{\partial t} - D\,\frac{\partial n(\ell',t)}{\partial x} \tag{8}$$

Equations (6), (7), and (8) contain so many unknown quantities that unfortunately they are of little use. However, they do show how various factors influence the pumping speed of sorbents. Sketches of the various flux rates in effect during sorption pumping are given in Fig. 3a.

2.2 DIFFUSION-LIMITED SORPTION

Dawbarn (Ref. 4) was the first to propose that diffusion alone may govern the sorption characteristics of frosts. He has suggested that once the desorption rate (i.e., re-evaporation) of molecules from a cryodeposit balances the adsorption rate, the pumping effect would cease unless molecules were able to diffuse into the frost. If adsorption-desorption equilibrium is established very rapidly, frost pumping by this process would be limited by the ability of molecules to diffuse into the cryodeposit.

In this case the term $[\partial N(\ell,t)]/\partial t$ in Eq. (7) rapidly approaches zero, which implies that the number of adsorbed molecules on the surfaces approaches a constant value resulting in a certain number density of molecules on the frost surface, n_o. As molecules diffuse into the cryodeposit, n_o is maintained constant by additional molecules being adsorbed onto the surface from the gas phase. This simplification is equivalent to neglecting the initial adsorption pumping transient as sketched in Fig. 3b. Any resulting solutions would be valid only after the surface is saturated with adsorbed molecules. Thus, in the special case where the sorption is diffusion-rate limited, one would solve Fick's second law,

$$\frac{\partial n(x,t)}{\partial t} = D\,\frac{\partial^2 n(x,t)}{\partial x^2} \tag{9}$$

for n(x,t), the distribution of diffused molecules in the cryodeposit at any time, assuming that the diffusion constant, D, is independent of n. The following initial and boundary conditions are appropriate to Dawbarn's diffusion-limited model:

1. $n(x,0) = 0$ (initially there are no sorbed molecules in the frost)
2. $n(\ell,t) = n_o$ = constant (the number of adsorbed molecules on the frost surface at $x = \ell$ is constant)
3. $\partial n(x,t)/\partial x]_{x=0} = 0$ (molecules do not penetrate the metallic cryosurface)

Assuming a product solution of the form $n(x,t) = X(x)\,T(t)$, Eq. (9) is easily solved by separation of variables. The solution with these boundary conditions is already available in the literature (Refs. 15 and 16) and takes the form

$$n(x,t) = n_o \left\{ 1 - \frac{4}{\pi} \sum_{n=o}^{\infty} \frac{(-1)^n}{(2n+1)} \cos\left[\frac{(2n+1)\pi x}{2\ell}\right] \exp\left[-\frac{(2n+1)^2\,\pi^2\,Dt}{4\ell^2}\right] \right\} \tag{10}$$

The flux of molecules diffusing away from the surface of the frost may be determined from Eq. (7) with $\partial N(\ell,t)/\partial t = 0$ which reduces to Fick's first law,

$$J = D \left.\frac{\partial n(x,t)}{\partial x}\right]_{x=\ell} \tag{11}$$

For the case of a perfect gas, this flux is related to the pumping speed by

$$S = J\left(\frac{kT_g}{P}\right)$$

Thus, for diffusion-limited pumping, the pumping speed is given by

$$S = \frac{2Dn_o\,k\,T_g}{P\ell} \sum_{n=o}^{\infty} e^{-(2n+1)^2\pi^2\,Dt/4\ell^2} \tag{12}$$

Equation (10) may also be used to derive an expression for the mean number of molecules sorbed per unit volume, which is an index of the sorption capacity of the frost,

$$n^* = \frac{1}{\ell} \int_a^{\ell} n(x,t)\,dx$$

Carrying out this integration results in

$$n^* = n_o \left\{ 1 - \frac{8}{\pi^2} \sum_{n=o}^{\infty} \frac{e^{-(2n-1)^2\pi^2\,Dt/4\ell^2}}{(2n+1)^2} \right\} \tag{13}$$

The limit of Eq. (13) as $t \to \infty$ shows that $n^*]_{max} = n_o$.

Thus, for this model molecules will diffuse into the frost until their number density throughout the frost is uniform and equal to the number density which can be adsorbed in equilibrium on the surface.

Calculations were carried out with Eqs. (12) and (13) to determine if they would predict at least the trends exhibited by available experimental data, such as given in Fig. 1. These equations, however, involve a factor which is not known: the diffusion constant for hydrogen or helium in solidified gases.

Ash, Barrer, and Pope (Ref. 17) report diffusion constants of about 10^{-4} cm^2/sec for the diffusion of nitrogen or argon in porous charcoal at about 77°K. Other

investigators have indicated that the self-diffusion constant of water in ice varies from about 10^{-12} cm^2/sec at 250°K (Ref. 18) to 10^{-17} cm^2/sec at 20°K (Ref. 19). Considering the lower cryodeposit temperatures employed in cryosorption pumping, one might expect the diffusion constants for hydrogen in cryofrosts to be anywhere from 10^{-8} to 10^{-20} cm^2/sec. Consequently, calculations were made for a wide range of values of D, as is shown in Fig. 4. It is observed that the theoretical curves do not agree with the observed experimental trends. The theoretical predictions would only appear to match the experimental observations in the range where the frost is nearly saturated with the sorbate gas, that is for the longer times. For reference purposes, the theoretical strike rate of hydrogen is also shown in Fig. 4. The pumping flux or speed could not exceed this value. Equation (12) cannot predict this trend because it does not have a limit as $t \rightarrow 0$. The trends of the experimental data suggest that during the initial stages of pumping, molecules can diffuse into the cryodeposit at a much faster rate than they can be sorbed, and initially the pumping is limited by some other mechanism. But, as more and more molecules are sorbed there is a decreasing concentration gradient in the frost (which is the potential that drives the diffusion process), and the process becomes diffusion-rate limited during the latter stages of pumping. Thus, it is believed that although the diffusion process suggested by Dawbarn plays an important role in frost cryosorption pumping, the overall process is much more complicated and involves at least one additional mechanism.

2.3 TWO-LAYER DIFFUSION MODEL

Since it was apparent that diffusion alone could not be responsible for the observed sorption pumping dynamics, a sorption pumping model which accounts for the penetration of adsorbed molecules into the frost as well as their subsequent diffusion through the frost is considered next.

This sorption model still assumes that molecules are adsorbed onto the surface and that the adsorption rate is not the limiting one. Then, they are assumed to migrate by diffusion into the disordered, porous interior of the frost, but in this case the diffusion process may be thought of as occurring in two steps:

1. diffusion away from the surface adsorption site, and

2. further diffusion into the pores, cracks, grain boundaries, etc., of the frost.

This model like the preceding one only accounts for diffusional processes; consequently, it is expected that it would best represent the more compact frost cryosorbents which are more likely to be diffusion-limited. As suggested previously and depicted by Fig. 2b, the diffusion barriers an adsorbed molecule must overcome to migrate away from its adsorption site are different from those which resist diffusion within the frost. Consequently, consistent with this model of sorption pumping, the cryosorbent frost is

divided into two regions: (1) a very thin layer near the surface with an effective thickness of ℓ_1 and (2) the remaining bulk frost layer of thickness ℓ_2 as sketched below.

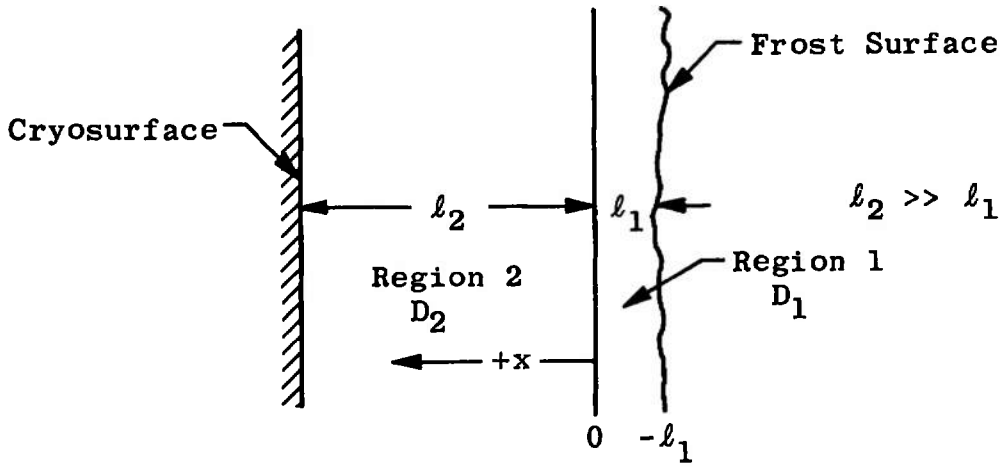

The thin surface layer (Region 1) is equivalent to a few monolayers in thickness (i.e., $\ell_1 \simeq 10^{-7}$ cm) and is assumed to have a diffusion constant D_1 which characterizes surface diffusion away from the adsorption surface. Region 2, the bulk of the frost layer, is assumed to possess a diffusion constant, D_2, which describes the diffusion process in the porous sorbent. Now, it is necessary to solve the diffusion equation for each region:

$$\frac{\partial n_1(x,t)}{\partial t} = D_1 \frac{\partial^2 n_1(x,t)}{\partial x^2} \tag{14a}$$

and

$$\frac{\partial n_2(x,t)}{\partial t} = D_2 \frac{\partial^2 n_2(x,t)}{\partial x^2} \tag{14b}$$

where n_1 and n_2 are the number densities of sorbed molecules in Regions 1 and 2, respectively. These two equations are coupled at the interface between the two regions, at x = 0, by the requirements that:

$$n_1(0,t) = n_2(0,t) \tag{15a}$$

$$D_1 \frac{\partial n_1(0,t)}{\partial x} = D_2 \frac{\partial n_2(0,t)}{\partial x} \tag{15b}$$

The remaining boundary conditions,

$$n_1(-\ell_1, t) = n_o \tag{15c}$$

$$\frac{\partial n_2(\ell_2,t)}{\partial x} = 0 \tag{15d}$$

and the initial condition,

$$n_1(x,0) = n_2(x,0) = 0 \tag{16}$$

are the same as employed previously and have already been adequately described, although a different coordinate system is used here.

The boundary conditions may be made homogeneous by letting

$$n' = n - n_o$$

The form of Eqs. (14a) and (14b) is unchanged by this transformation; n is just replaced by n′, whereas Eqs. (15) and (16) become

$$n_1'(0,t) = n_2'^{1}(0,t) \tag{17a}$$

$$D_1 \frac{\partial n_1''(0,t)}{\partial x} = D_2 \frac{\partial n_2^{1}(0,t)}{\partial x} \tag{17b}$$

$$n_1'(-\ell_1,t) = 0 \tag{17c}$$

$$\frac{\partial' n_2(\ell_2,t)}{\partial x} = 0 \tag{17d}$$

and

$$n_1'(x,0) = n_2'(x.0) = -n_o \tag{18}$$

Equation (14) may be solved by separation of variables, and the details of this solution which could not be found in the literature are contained in Appendix II. The solution takes the form of:

$$n_1(x,t) - n_o = \sum_{n=1}^{\infty} A_1^{(n)} \left[\frac{\sin \lambda_1^{(n)}(x+\ell_1)}{\sin \lambda_1^{(n)}\ell_1}\right] e^{-\lambda_1^{(n;2} D_1 t} \tag{19a}$$

$$n_2(x,t) - n_o = \sum_{n=1}^{\infty} A_1^{(n)} \left[\frac{\cos \lambda_2^{(n)}(x-\ell_2)}{\cos \lambda_2^{(n)}\ell_2}\right] e^{-\lambda_2^{(n)2} D_2 t} \tag{19b}$$

where the Fourier coefficients $A_1^{(n)}$ are given by:

$$A_1^{(n)} = -\left[\frac{2 D_1 n_o}{\lambda_2^{(n)}}\right]\left[\frac{\sin \lambda_2^{(n)}\ell_2 \cos \lambda_2^{(n)}\ell_2 \cos \lambda_1^{(n)}\ell_1}{\ell_1 D_2 \sin^2 \lambda_2^{(n)}\ell_2 + D_1\ell_2 \cos^2 \lambda_1^{(n)}\ell_1}\right] \tag{20}$$

and the eigenvalues $\lambda_1^{(n)}$ and/or $\lambda_2^{(n)}$ are obtained from

$$\cot(\lambda_1^{(n)}\ell_1) = \frac{D_2\lambda_2^{(n)}}{D_1\lambda_1^{(n)}} \tan(\lambda_2^{(n)}\ell_2) \tag{21}$$

and

$$(\lambda_1^{(n)})^2 D_1 = (\lambda_2^{(n)})^2 D_2 \tag{22}$$

Equations (19) through (22) specify the distribution of sorbed molecules in Regions 1 and 2; however, they involve four quantities, ℓ_1, ℓ_2, D_1, and D_2. Since $\ell_1 << \ell_2$, ℓ_2 may be assumed equal to the frost thickness. In addition, the final equilibrium number density, n_o, must be given, but it may be obtained from measured or calculated equilibrium isotherms available in Refs. 10 and 11.

2.3.1 Approximation for Small ℓ_1

Because ℓ_1 is very small, the number of sorbed molecules ultimately stored in this layer is quite small compared to the number which may be stored in the rest of the frost. Without great loss in generality, one may simplify the preceding solution for the case of an infinitesimal surface layer ℓ_1.

By inverting Eq. (21), one obtains

$$\sqrt{\frac{D_2}{D_1}} \tan\sqrt{\frac{D_2}{D_1}}\,\lambda_2^{(n)}\ell_1 = \cot(\lambda_2^{(n)}\ell_2')$$

Then, for small values of $\sqrt{D_2/D_1}\ \lambda_2^{(n)}\ell_1$, which will occur for infinitesimal values of ℓ_1, the tangent of the angle is approximated by the angle

$$\tan\left(\sqrt{\frac{D_2}{D_1}}\,\lambda_2^{(n)}\ell_1\right) \simeq \sqrt{\frac{D_2}{D_1}}\,\lambda_2^{(n)}\ell_1$$

and the characteristic equation becomes

$$\ell_2\lambda_2^{(n)} = \left(\frac{D_1}{\ell_1}\right)\left(\frac{\ell_2}{D_2}\right)\cot(\lambda_2^{(n)}\ell_2) \tag{23}$$

Similarly, the limit of $A_1^{(n)}$ [Eq. (20)] for small values of ℓ_1 may be obtained by successive application of l'Hospital's Rule, and results in,

$$A_1^{(n)} = \frac{-n_o \sin(2\lambda_2^{(n)}\ell_2)}{\lambda_2^{(n)}\ell_2 + \dfrac{\sin(2\lambda_2^{(n)}\ell_2)}{2}} \tag{24}$$

Now an approximate expression for $n_2(x,t)$ may be written,

$$n_2(x,t) = n_o - n_o \sum_{n=1}^{\infty} \frac{2e^{(-\lambda_2^{(n)2} D_2 t)} \sin(\lambda_2^{(n)} \ell_2) \cos[\lambda_2^{(n)} (\ell_2 - x)]}{\lambda_2^{(n)} \ell_2 + \frac{\sin(2\lambda_2^{(n)} \ell_2)}{2}} \tag{25}$$

where the characteristic values of $\lambda_2^{(n)}$ are obtained from the roots of Eq. (23). These roots have been tabulated by Carslaw and Jaeger (Ref. 20). The existence of the surface layer has not disappeared in the solution inasmuch as the ratio (D_1/ℓ_1) is still contained in Eq. (23). With this simplification only two quantities must be provided, D_2 and (D_1/ℓ_1). The latter ratio still represents the notion that the diffusion barrier near the surface is different than that which characterizes the interior of the sorbent.

2.3.2 Another Viewpoint

Smits and Miller (Ref. 21) have solved Fick's second law for conditions which correspond to the diffusion of impurities in semiconductors. They considered a semi-infinite medium with a boundary condition that specified the existence of a mass transfer coefficient at the surface. Smith (Ref. 22) and Boltaks (Ref. 23) have examined this solution further and found that it agreed with experimental results. A sorption pumping model may be formulated in a similar way.

Fick's second law,

$$\frac{\partial n(x,t)}{\partial t} = D \frac{\partial^2 n(x,t)}{\partial x^2}$$

is again solved but with the conditions that

1. At the cryosurface, $x = \ell$, $\quad \partial n(\ell,t)/\partial x = 0$
2. At the frost surface, $x = 0$ $\quad D\partial n(0,t)/\partial x = G[n_o - n(0,t)]$
3. Initially, $t = 0$, $n(x,0) = 0$

The boundary condition at the frost surface states that the flux of molecules across the surface is proportional to the difference in the sorbed particle number densities just inside the frost $[n(0,t)]$ and just outside the frost in an adsorbed layer (n_o). The proportionality constant, G, is an undefined mass transfer coefficient.

The solution with this set of boundary conditions is already available (Ref. 16) and takes the form

$$n(x,t) = n_o - n_o \sum_{n=1}^{\infty} \frac{2e^{-\lambda^{(n)2} D t} \sin(\lambda^{(n)} \ell) \cos(\lambda^{(n)} (\ell - x))}{\lambda^{(n)} \ell + \frac{\sin(2\lambda^{(n)} \ell)}{2}} \tag{26}$$

where $\lambda^{(n)}$ values are obtained from the characteristic equation

$$\lambda^{(n)}\ell = \frac{G\ell}{D} \cot(\lambda^{(n)}\ell) \tag{27}$$

It is evident by comparison of Eqs. (26) and (27) and Eqs. (25) and (23) that the "small ℓ_1" approximation of the two-layer diffusion model is equivalent to a mass transfer coefficient model, where the surface mass transfer coefficient is defined by

$$G \equiv \frac{D_1}{\ell_1}$$

This suggests that a thin surface layer may act as a barrier and govern the mass transfer of the sorbate into the frost.

2.3.3 Generalized Equations

A dimensionless parameter occurs in the characteristic equation (Eq. 23)

$$N_D = \frac{(D_1/\ell_1)\,\ell_2}{D_2}$$

It may be interpreted physically as the ratio of internal resistance to surface resistance and is analogous to the Biot modulus which is frequently encountered in heat transfer. It will be referred to here as the diffusion Biot number. Also, the Fourier modulus

$$N_F = \frac{Dt}{\ell^2}$$

could be employed to nondimensionalize the time. In terms of these dimensionless groups, Eq. (23) becomes

$$\ell_2\lambda_2^{(n)} = N_D \cot(\lambda_2^{(n)}\ell_2) \tag{28}$$

and substituting it into Eq. (25) results in

$$\frac{n_2(x,t)}{n_o} = 1 - \sum_{n=1}^{\infty} \frac{2e^{-(\lambda_2^{(n)}\ell_2)^2 D_2 t/\ell_2^2} \sin^2(\lambda_2^{(n)}\ell_2) \cos\left[\lambda_2^{(n)}\ell_2\left(1 - \frac{x}{\ell_2}\right)\right]}{N_D \cos(\lambda_2^{(n)}\ell_2) + \sin^2(\lambda_2^{(n)}\ell_2) \cos(\lambda_2^{(n)}\ell_2)} \tag{29}$$

Expressions for the pumping speed and sorption capacity may be obtained from Eq. (29), since

$$J = -D_2 \left.\frac{\partial n_2(x,t)}{\partial x}\right]_{x=0} \tag{30}$$

and

$$n^* = \frac{1}{\ell_2}\int_0^{\ell_2} n_2(x,t)\,dx \tag{31}$$

Carrying out these operations yields

$$\frac{J}{n_o(D_1/\ell_1)} = 2 \sum_{n=1}^{\infty} \frac{\sin^2(\lambda_2^{(n)}\ell_2)\, e^{-(\lambda_2^{(n)}\ell_2)\, D_2 t/\ell_2^2}}{N_D + \sin^2(\lambda_2^{(n)}\ell_2)} \tag{32}$$

and

$$\frac{n^*}{n_o} = 1 - 2 \sum_{n=1}^{\infty} \frac{\sin^2(\lambda_2^{(n)}\ell_2)\, \tan^2(\lambda_2^{(n)}\ell_2)\, e^{-(\lambda_2^{(n)}\ell_2)2\, D_2 t/\ell_2^2}}{N_D(N_D + \sin^2(\lambda_2^{(n)}\ell_2))} \tag{33}$$

The dynamic variation of (1) the sorbed particle distribution in the sorbent, (2) the pumping speed, and (3) the capacity may be calculated from Eqs. (29), (32), and (33), respectively. It is necessary to specify the sorbent thickness, ℓ_2, and the final equilibrium number density, n_o. The first is a controllable experimental parameter, and the latter may be obtained from equilibrium sorption isotherms (Ref. 10) because at $t \to \infty$, Eq. (33) shows that $n^* \to n_o$. In addition, values of D_2 and the ratio (D_1/ℓ_1) must be specified.

2.3.4 Analytical Calculations

Calculated distributions [Eq. (29)] of the sorbate molecules in the sorbent are given in Fig. 5 with the Fourier modulus (dimensionless time) as a parameter. Two different cases are shown and both illustrate that a large sorbed particle number density gradient exists across the infinitesimally thin surface layer. The distributions in Fig. 5a correspond to a diffusion Biot number of $N_D = 10$, i.e., the internal resistance to diffusion is ten times the surface resistance, whereas the Fig. 5b distributions illustrate the situation in which the surface resistance is much larger than the internal resistance, $N_D = 10^{-2}$. In this latter case $D_2 = 10^{-8}$ cm^2/sec, and it is evident that once the molecules diffuse away from the surface, they have little difficulty in migrating through the frost. For lower diffusion constants, for example when $D_2 = 10^{-11}$ cm^2/sec (Fig. 5a), the internal resistance is sufficiently high to support large concentration gradients during the initial stages of pumping.

A systematic series of calculations of the sorbed particle flux [Eq. (32)] and the sorption capacity [Eq. (33)] have been made and are summarized in Fig. 6. The diffusion Biot number is employed as a parameter in this presentation. It is observed that for $N_D \ll 1$ the calculated curves have the same general trend as the various measured dynamic pumping curves shown in Fig. 1. Values of the diffusion Biot number less than unity correspond to the case where the forces resisting diffusion away from the sorbent surface are greater than those resisting diffusion within the sorbent. With increasing Biot number internal diffusion dominates, and the calculated dynamic pumping curves are similar to those obtained from the diffusion-limited model derived previously and shown in Fig. 4. At low values of the diffusion Biot number the calculated curves appear to approach a limit which is not immediately evident by inspection of Eqs. (32) and (33) because of their complexity. However, for the case where the sorption process is controlled solely by the surface resistance, diffusion effects may be neglected and Eq. (7) shows that

$$J_p = \frac{1}{A_f} \frac{dN(\ell, t)}{dt}$$

But, the equivalent number density of adsorbed molecules on the surface is equal to the number density of sorbed molecules since there are no gradients in the sorbent (i.e., dn/dx = 0). Hence, this expression may be written

$$J_p = \ell_2 \frac{dn(t)}{dt}$$

If a mass transfer coefficient $G = D_1/\ell_1$ is assumed at the surface to represent the surface resistance, then[1]

$$\ell_2 \frac{dn(t)}{dt} = \frac{D_1}{\ell_1} (n_o - n(t))$$

which, when solved with the initial condition that n = 0 at t = 0, results in

$$n = n_o (1 - e^{-(D_1/\ell_1)t/\ell_2}) \tag{34}$$

Since the particle flux is

$$J_p = \ell_2 \frac{dn(t)}{dt}$$

and the sorption capacity is

$$n^* = \frac{1}{\ell_2} \int_o^t J_p \, dt$$

Equation (34) may be used to show that in the limit of negligible internal resistance,

$$\frac{J_p}{n_o(D_1/\ell_1)} = e^{-(D_1/\ell_1)t/\ell_2}$$

and

$$\frac{n^*}{n_o} = 1 - e^{-(D_1/\ell_1)t/\ell_2}$$

These two equations may be combined to show this limiting case of negligible internal resistance corresponds to

$$\frac{n^*}{n_o} = 1 - \frac{J_p}{n_o(D_1/\ell_1)} \tag{35}$$

The limit given by Eq. (35) is also shown in Fig. 6 and is observed to be the limit of Eqs. (32) and (33) as N_D approaches zero.

2.4 ADSORPTION-RATE LIMITED CASE

It is difficult to analyze the sorption process when it is limited by the rate at which molecules are adsorbed on the surface. The difficulties center about the unknown nature of the surface and lack of practical information concerning the details of

[1]This case corresponds to that of Newtonian heating in an analogous heat-transfer problem; see Ref. 16 for details.

gas-surface interaction, and in particular the sticking probability and desorption characteristics. The present test results and Ref. 11 give at least some information about these factors.

The equilibrium isotherm curves given in Ref. 11 and typically shown here in Fig. 7 may be cross-plotted in the form of isosteres, and then the desorption energy can be obtained from the Clausius-Clapeyron equation,

$$E_d\,(C) = 4.57 \left.\frac{d(\ln P)}{d(1/T_f)}\right]_C \quad \text{cal/mole} \tag{36}$$

where P is in torr and T_f is in °K. The results of such calculations are given in the following table:

	E_d, cal/mole		
Equilibrium Capacity, C	$\dot{n}_{form} = 6.3 \times 10^{15}$	$\dot{n}_{form} = 6.3 \times 10^{16}$	$\dot{n}_{form} = 3.15 \times 10^{17}$
0.05	1320	1360	1375
0.10	1165	1295	1320
0.15	1050	1240	1265
0.20	970	1170	1215
0.30	---	1050	1115

Note that E_d decreases with increasing equilibrium capacity, C. This characteristic is exhibited by a variety of porous sorbents (see Ref. 5, for example), and according to Eq. (6) it would result in a decrease of the pumping speed with increasing quantity of gas sorbed. However, calculation of the increase of the re-evaporated flux caused by the decrease of desorption energy shown in the above table has shown that the variation of E_d with the amount of gas sorbed cannot solely account for the observed decrease in pumping speed. Examination of the experimental data (such as Fig. 1) indicates that the sticking probability, c, must also decrease with an increasing quantity of gas sorbed (i.e., $c = c(N(t))$.

Adsorption could be the rate-limiting process if the frost possesses extremely high diffusion constants. In this case the diffusion term in Eq. (8) is neglected (as in the preceding treatment), but now the remainder of Eq. (8) must be solved.

$$\frac{dN(t)}{dt} = \frac{A_f\, c\,(N(t))\, P}{\sqrt{2\pi m k T_g}} - \frac{N(t)}{\tau} e^{-E_d(N(t))/kT_f} \tag{37}$$

To obtain the preceding solutions it was assumed that the number of adsorbed molecules on the surface was constant. A solution to this equation, however, would specify how the number of adsorbed molecules would vary with time. In general, a closed-form solution is not possible. First, the sticking probability, c, and desorption energies, E_d, are unknown functions of the amount of gas sorbed. Second, since Eq. (37) is nonlinear, even if these

functions were known a closed-form solution is probably still impossible. In any case Eq. (37) may be used to determine the proper time-dependent boundary condition to represent the adsorption-rate limited case.

No attempt was made here to derive a mathematical model for this adsorption-rate limited mechanism A realistic model probably cannot be established until the gas-surface interaction problem is better understood. As a result one must turn to experimentation to determine the complex variation of the sticking probability, sorption energy, and adsorption characteristics.

SECTION III
EXPERIMENTAL APPARATUS AND CALIBRATIONS

3.1 CHAMBER AND PUMPING SYSTEM

The 36-in.-high by 30-in.-diam stainless steel vacuum chamber used for cryosorption of hydrogen is schematically shown in Fig. 8. Its pumping system consists of a mechanical roughing pump and a 6-in. oil diffusion pump which is equipped with a liquid-nitrogen-cooled baffle and has a pumping speed of 1500 liters/sec. A 6-in. high-vacuum, air-operated gate valve is used to isolate the chamber from the pumping system. Access to the chamber is achieved by means of a removable top which employs an O-ring seal. The chamber base pressure without bakeout was between 5×10^{-7} and 1×10^{-7} torr.

A 25-in.-high by 24-in. diam stainless steel shroud was installed in the chamber. It was constructed from overlapping slats (see Fig. 8) in a manner to allow free passage of the molecules, but was optically tight. The shroud was maintained at room temperature for all of the hydrogen sorption tests. The cryosorption pump was centrally located inside the shroud, and together with the shroud was attached to the removable chamber top. After correcting for the space occupied by the shroud, sorption pump and other items the chamber had a free volume of 300 liters.

3.2 CRYOSORPTION PUMP

The cryosurface upon which the frost sorbent was deposited was a 6-in.-diam stainless steel sphere with an available pumping area of 970 cm^2. It was attached to a vacuum-jacketed, concentric, gaseous helium supply and return line which was installed in the removable lid. This concentric line was in turn plumbed directly to a helium refrigerator via vacuum-jacketed transfer lines. The refrigerator was a modified Collins cryostat which had about 180 watts of refrigeration capacity and supplied gaseous helium in the temperature range from 12 to 70°K.

3.3 GAS ADDITION SYSTEM

Hydrogen and the various gases predeposited to form the sorbents were obtained from commercially available high-pressure bottles. These gases were introduced into the top of the chamber in the region between the shroud and chamber wall by means of two

gas addition systems. Generally, one system was used to add the sorbent gas and the other to add hydrogen. Methods used to calibrate the leaks are described in Ref. 10.

It was not possible to measure directly either the sorbent thickness or its uniformity. However, since the gas molecules would have to have many collisions with the chamber walls and baffles before they could pass through the optically tight shroud, it is believed that the molecules struck the pumping surface randomly from every direction. As a check, however, both the sorbent gas and hydrogen were introduced sequentially into the chamber at the same point, for some of the tests. If the particle ballistics were such that more sorbent was deposited in one place than another, then the hydrogen would also strike at a higher rate in these same regions. However, the test results appear unaffected by the gas addition location. After the sorbent had been added on the pumping surface at temperatures below 20°K and before the hydrogen addition was started, the base pressure decreased to about 1×10^{-8} to 4×10^{-8} torr.

3.4 INSTRUMENTATION

An ion gage and a magnetic-deflection-type mass spectrometer were used to measure the pressures in the chamber (see Fig. 8). Tubulation inside the chamber was employed to prevent the gages from directly sensing the pumping surface, and oriented so that the gages would sense about the same flux of particles as the pumping surface. The time constant of the tubulation has been calculated to be 3.8×10^{-6} sec for 300°K hydrogen (Ref. 4). For higher pressure tests the ion gage was replaced with an Alphatron®. Ion gage and mass spectrometer outputs were recorded on strip charts with time as a variable. The pressure on the high-pressure side of the porous plug leaks in the gas addition system was monitored with a conventional bellows-type gage, and recorded by means of a transducer and a strip chart recorder. Techniques used to calibrate the pressure instrumentation in place before each series of tests are given in Ref. 10.

A hydrogen vapor-pressure thermometer was used to determine the temperature of the gaseous-helium-cooled surfaces at temperatures between 10 and 25°K. At higher temperatures a helium gas thermometer was employed. The bulbs of both of these devices were located inside of the sorption pump and heliarc welded into holes in the pumping surface. Iron oxide was used in the bulb of the hydrogen vapor thermometer as a catalyst to promote conversion to parahydrogen. The hydrogen vapor pressure was measured with a 0- to 100-psia gage having a low internal volume and used to obtain temperatures from hydrogen vapor pressure curve. The thermometer had previously been calibrated at 20.4°K by submerging the bulb in liquid hydrogen at atmospheric pressure. Temperatures measured with the hydrogen vapor thermometer were quite close to the arithmetic mean temperature in the refrigerated helium in the supply and return lines. It is assumed that the surface temperature of the frost was closely approximated by the bulb temperature. Temperatures obtained with the hydrogen vapor thermometer are believed to have been accurate to ±0.5°K in the range between 12 and 25°K.

A helium gas thermometer used to measure higher frost temperatures was calibrated against the hydrogen vapor pressure thermometer in the range from 12 to 25°K. This calibration curve (see Ref. 10) was extrapolated to higher temperatures as

guided by the mean temperature in the gaseous-helium supply and return lines. Temperatures between 25 and 40°K are believed to have been accurate within ±2°K. Above 40°K, measured temperatures are believed to have been accurate to within ±5°K.

SECTION IV
PROCEDURES AND CALCULATIONS

4.1 SORPTION TEST PROCEDURES

Prior to each series of sorption pumping runs, the molecular leak and pressure gage calibrations were carried out by the methods described in Ref. 10. All runs were started by pumping the chamber to its base pressure level by the diffusion pump. The two gas addition systems were evacuated by their pumping systems and flushed several times with the gas to be used.

Next, the cryosurface was cooled by circulating cold gaseous helium from the cryostat through it. Its temperature was monitored by the hydrogen vapor thermometer and the supply and return temperatures at the refrigerator. At the maximum refrigerator capacity the cryosurface could be maintained at 12°K. By bypassing a portion of the cold helium, the cryosurface temperature could then be adjusted to the desired temperature. When this temperature was reached, the chamber was isolated from its pumping system and ready for admission of the sorbent gas.

4.1.1 Formation of Sorbent Frost

All of these tests were conducted by predepositing the frost sorbent before beginning the addition of hydrogen. The sorbent gases used for these tests and their purities as given by the manufacturer (Matheson Chemical Co.) are listed in the following table:

Sorbent	Purity, percent
Carbon Dioxide	99.99
Sulphur dioxide	99.90
Methyl chloride	99.50

The reservoir of the sorbent gas addition system was filled to a particular forepressure which established the sorbent addition rate for a given leak. As the sorbent gas was admitted into the isolated chamber, the pressure rose to a level which depended upon the forepressure. Some typical values of conditions at which the carbon dioxide frost was formed are summarized below:

Chamber Pressure, torr	Carbon Dioxide Strike Rate, molecules/cm^2-sec	Mean Frost Growth Rate $\overline{d\ell/dt}$, μ/min
2×10^{-6}	6.3×10^{14}	0.0045
2×10^{-5}	6.3×10^{15}	0.045

Chamber Pressure, torr	Carbon Dioxide Strike Rate, molecules/cm^2-sec	Mean Frost Growth Rate $d\bar{\ell}/dt$, μ/min
2×10^{-4}	6.3×10^{16}	0.45
1×10^{-3}	3.15×10^{17}	1.0

Most of the sorbents were formed at different chamber pressure levels or strike rates by varying the leak forepressure. However, a few were formed by pumping the chamber to its base pressure and then backfilling it with helium to pressures as high as 10^{-1} torr. The sorbent gas was then introduced into the chamber and the sorbent formed at relatively high helium partial pressure levels. Both the leak forepressure and chamber pressures were recorded continuously and held constant during the prescribed addition time. Afterward, the helium was removed from the chamber by the diffusion pump.

The forepressure and the leak calibration allowed measurement of the amount of sorbent added, Q_s. For convenience of discussion, the mean thickness of the sorbent frost was estimated from Q_s, assuming that all of the sorbent gas added to the chamber was deposited on the cryosurface.

$$m_s = \frac{Q_s m_g}{k T_g} = m_f = \rho_f A_f \bar{\ell}_f$$

or

$$\bar{\ell}_f = \frac{Q_s m_g}{A_f \rho_f k T_g} \tag{38}$$

The density of the frost is needed to estimate the frost thickness. Densities of some species of frost used for these tests are available, but the densities of others had to be estimated from the published values of their liquid density and the general trends between liquid and frost densities.

Sorbent	ρ_{liq}, gm/cm^3	ρ_f, gm/cm^3
Carbon dioxide	1.19 (Ref. 24)	1.60 (Ref. 25)
Nitrogen	0.804 (Ref. 24)	0.90 (Ref. 26)
Argon	1.41 (Ref. 24)	1.77 (Ref. 27)
Sulphur dioxide	1.46 (Ref. 24)	1.80 (Estimated)
Methyl chloride	1.00 (Ref. 24)	1.20 (Estimated)

Sorbent thicknesses from 0.1 to 4 microns were achieved by varying the flow rate and time of the sorbent addition.

4.1.2 Kinetic Pumping Measurements

Once the frost was deposited, the sorbate gas was admitted to the chamber through its gas addition system; the chamber remained valved off from its pumping system. Two different sorbate addition techniques were used.

Constant Sorbate Flow Rate – The leak forepressure was held constant during the addition to maintain the sorbate addition rate constant at some desired value. Typical time histories of the chamber pressure and sorbate forepressure for this mode of operation are given in Fig. 9. Preliminary tests demonstrated that when the chamber pressure had increased to about 3×10^{-4} torr, the frost sorbent was essentially saturated with the sorbate and its pumping speed was reduced to a few liters per second. This will be referred to hereafter as the saturation pressure. The test runs were terminated at this point by shutting off the sorbate flow.

Variable Sorbate Flow Rate – For this operational mode, the forepressure in the sorbate leak system was initially set at some value and the flow started which resulted in some corresponding value of the chamber pressure. Then, as the pumping speed of the frost characteristically decreased as it sorbed hydrogen, the forepressure on the leak and, hence, the sorbate flow rate were steadily decreased in a manner to maintain a constant chamber pressure. The test was completed when the sorbate forepressure was reduced to zero. Forepressure and chamber pressure time histories for this mode of operation are presented in Fig. 10.

4.2 CALCULATIONAL PROCEDURES

4.2.1 Pumping Speed

The definition of pumping speed has not been used in a consistent manner in the cryosorption literature. For example, Southerlan (Ref. 3), Dawbarn (Ref. 4), and Yuferov and Busol (Ref. 5) have each defined and calculated the pumping speed of frost sorbents in different ways. Other investigators have avoided the problem of defining the pumping speed by presenting only the chamber pressure histories during sorption tests.

The speed of a pump is generally defined as the volume of gas removed from the chamber per unit time at the existing pressure level. Then, the total gas load or throughput handled by the pump is the product of the pumping speed and the pressure at the pump inlet:

$$\dot{Q} = PS$$

It is also given by

$$\dot{Q} = \dot{Q}_{add} + \dot{Q}_{out} - V_c \frac{dP}{dt}$$

where $\dot{Q}_{add}$ represents the intentionally added sorbate gas load, $\dot{Q}_{out}$ is the gas load attributable to chamber outgassing and leakage, and $V_c(dP/dt)$ represents the amount of gas which enters the chamber volume but is not pumped. If gas is not being intentionally added to the chamber ($Q_{add} = 0$), the pump will reduce the chamber pressure to its ultimate value which would be fixed by outgassing and leakage. Thus, $\dot{Q}_{out}$ is given by

$$\dot{Q}_{out} = P_u S$$

Combining these expressions results in

$$S = \frac{\dot{Q}_{add} - V_c \frac{dP}{dt}}{(P - P_u)} \tag{39}$$

Equation (39) has been employed to calculate the pumping speeds presented here. To provide meaningful values the pressure measurement location was such that it sensed the flux of molecules striking the sorption surface. Values of dP/dt were obtained by manually taking the slopes of a pressure-time plot, and $\dot{Q}_{add}$ was determined from

$$\dot{Q}_{add} = P_a K$$

4.2.2 Frost Sorption Capacity

The amount of gas pumped by a frost sorbent or a molecular sieve has also been reported in a variety of ways. A nondimensional method is employed here.

The amount of gas added to the chamber to form the sorbent was computed from

$$Q_{sorbent} = t\,[P_a K]_{sorbent} \tag{40}$$

where Q has dimensions of torr-liters. When the sorbate was added at a constant rate, the amount added may be similarly determined from

$$Q_{sorbate}]_{P_s = const} = t[P_a K]_{sorbate} \tag{41a}$$

For tests where the sorbate addition rate was varied to hold the chamber pressure constant the amount of sorbate gas was computed from

$$Q_{sorbate}]_{P_c = const} = [K]_{sorbate} \int_0^t P_a(t)dt \tag{41b}$$

The integration was carried out manually on figures such as Fig. 10 by use of a planimeter.

The sorption capacity of the frost is defined as

$$C \equiv \frac{Q_{sorbate}}{Q_{sorbent}} \tag{42}$$

The quantity C is referred to as the "mole ratio" by some investigators (Refs. 4, 7, and 8) and as the "concentration" by others (Refs. 5 and 9). It is merely a convenient nondimensional way to express the amount of gas which has been sorbed and is referred

to here as the capacity of the frost. The value of C at the saturation pressure is referred to as the saturation capacity.[2]

SECTION V
DISCUSSION

5.1 HYDROGEN PUMPING SPEED MEASUREMENTS

The pumping speed of the "bare" cryosurface at a temperature of 12.4°K is given in Fig. 11a. It appears that the stainless steel surface has a high pumping speed for several seconds and sorbs appreciable quantities of hydrogen. However, this is not the true picture; the surface is actually covered with a thin but unknown amount of cryodeposit from the residual and desorbed gases in the chamber. This is demonstrated by the fact that the chamber pressure decreases about a decade as the cryosurface is cooled to 12°K. Consequently, the "bare" surface pumping effect is due to cryosorption.

Dynamic pumping speed curves for 12.4°K carbon dioxide frost layers of three different thicknesses, but otherwise formed in the same manner, are also shown in Fig. 11a. The curves are displaced by time intervals which are proportional to the frost thickness. Consequently, if these data are replotted in terms of the dimensionless capacity parameter, C, they produce essentially a single pumping curve as shown in Fig. 11b.

A similar series of sorption pumping curves is given in Fig. 12a in which the sorbate flow rate was varied in order to maintain a constant chamber pressure during sorption. Because the sorbate flow rate is continuously decreasing, the pumping speed is shown as a function of the amount of hydrogen sorbed. Again, on the basis of the dimensionless frost capacity the pumping curves collapse into essentially a single curve (Fig. 12b), although the scatter is somewhat greater particularly in the vicinity of the knee in the curve.

The trends shown in these figures are similar to those obtained by Hunt, et al. (Ref. 2) for the sorption of hydrogen by a carbon dioxide frost (Fig. 1). The pumping speed of carbon dioxide frost always decreases rather slowly from its initial value as hydrogen sorbed. Although it appears on the log plots that the pumping speed is constant for some time, it actually always decreases steadily as the capacity increases. Then it falls off very rapidly as saturation is approached. The present tests further illustrate two important points.

First, the initial pumping speed of the frost is completely independent of the volume of the frost. Additional tests with a cryosurface of different geometry and the pumping speed results of other investigators show that the initial pumping speed is proportional to the geometric surface area of the frost. Thus, while the sorption capacity is governed by the volumetric or bulk characteristics of the frost (see Ref. 10), the initial

[2]The volume of gas sorbed in cubic centimeters at standard pressure and temperature divided by the mass of the sorbent in grams is also quite frequently used in the isotherm and molecular sieve literature to describe the quantity of gas sorbed by a porous medium. This parameter is analogous to the factor C employed here.

pumping speed depends primarily on the interaction of the sorbate molecules with the sorbent surface. The nature of the complex sorbate-sorbent interaction is discussed later. The subsequent decrease of the pumping speed as the frost approaches saturation is governed by one or more of the rate limiting processes mentioned at the beginning of Section II.

Secondly, several investigators have found that at equilibrium, the amount of hydrogen sorbed by a carbon dioxide frost was directly related to the frost volume (or thickness for a given frost surface area). The dynamic pumping curves (Figs. 11 and 12) further demonstrate the important fact that this situation exists throughout the pumping process. Consequently, a pumping speed curve measured for a frost at one thickness can be used to estimate the dynamic pumping characteristics of frosts formed at the same conditions but having different thicknesses.

5.1.1 Effect of Frost Temperature

Pumping speed versus capacity curves for carbon dioxide frosts formed at two pressure levels and temperatures are given in Fig. 13. Higher temperature frosts are observed to have lower initial pumping speeds. This agrees with pumping speed data obtained previously by Dawbarn (Ref. 4) and is associated with a higher desorption rate of the warmer frosts. The present tests, however, more completely characterize the pumping process for different frost temperatures. They demonstrate that as the frost temperature increases, the capacity range, or time interval over which the pumping speed is constant, is reduced.

5.1.2 Effect of Frost Formation Rate

Dynamic pumping speed curves for frosts formed at various strike rates are summarized in Fig. 14. Note that linear coordinates are employed here to better illustrate the differences in pumping characteristics of the different frosts. Forming the frost at a higher rate, which as shown previously (Ref. 10) made it more disordered and increased its equilibrium capacity, also resulted in a small decrease in its initial pumping speed. This trend was also exhibited by higher temperature frosts (for example, compare T_f = 21.5°K and T_f = 16.5°K curves in Fig. 13).

Figure 14 also illustrates that the more porous frosts formed at higher strike rates have relatively constant pumping speeds over a wide range of their sorption capacity. It is apparent that the advantage gained in increased sorption capacity by forming a porous frost greatly outweighs the modest decrease in pumping speed.

5.1.3 Effect of Warming the Frost

It was previously demonstrated in Ref. 10 that intermediate warming of the frost decreased its equilibrium sorption capacity. Figure 15 further shows that, when a frost is cycled through some temperature range, its dynamic pumping speed curves are essentially shifted to lower capacity, but warming the frost also produces a small increase of the initial pumping speed. Although an intermediate increase of the frost temperature may

grossly alter its structure, it obviously does not significantly alter the interaction character of its surface, as indicated by its initial pumping rate.

5.1.4 Different Sorbents

Dynamic pumping speed curves for sulphur dioxide and methyl chloride sorbents are compared to that of carbon dioxide in Fig. 16. All of these frosts were formed at essentially the same conditions. All of the curves have similar shapes but somewhat different values of initial pumping speed and saturation capacity. The methyl chloride frost exhibited the highest pumping speed of those investigated in this study.

5.1.5 Comparison with Other Investigators

Unit pumping speeds of about 30 liters/sec-cm^2 measured during this investigation for carbon dioxide frost appear to be somewhat greater than those published by other investigators (see Refs. 2, 4, and 5). The differences, however, are largely due to the way in which the pumping speed is defined. The fact that in a closed chamber the frost is also pumping a gas load caused by outgassing and inleakage has not always been considered. Equation (39), employed to compute all of the pumping speeds presented here, credits the frost for handling this additional gas load and more realistically represents the true frost pumping speed. Others have generally reported "system" pumping speeds, and the present pumping speed results are actually quite consistent with those obtained previously. The shape of the dynamic pumping curves are quite similar to those obtained by Hunt, et al. (Ref 2, and given in Fig. 1) and Yuferov and Busol (Ref. 5), and the reduction in pumping speed attendant to higher frost temperatures as previously noted by Dawbarn (Ref. 4) was also verified.

There is one notable difference between the shapes of most of the dynamic pumping speed curves obtained during this investigation and those obtained previously (Refs. 2 and 5). Frosts formed at strike rates greater than about 10^{15} molecules/cm^2-sec exhibited slowly decreasing pumping speeds over a wide range of sorption capacity (see Fig. 14). As the saturation point was approached, the pumping speed fell off abruptly. In contrast, frost sorbents formed at lower strike rates by other investigators (see Fig. 1), as well as at the one formed at the lowest strike rate employed for these tests, had pumping speeds which tended to decrease rapidly during the initial stages of pumping. These differences are believed to be due to the difference in the structural properties of the frost.

The theoretical strike rate of 300°K hydrogen on a surface corresponds to an equivalent maximum pumping speed of about 44 liters/sec-cm^2. This implies that the maximum effective capture coefficient of the carbon dioxide frost for hydrogen varies between about 0.55 and 0.70 for the various kinds of frost structures formed in this investigation. These values are in the same range as those reported previously (Ref. 1).

No other investigators have examined sulphur dioxide or methyl chloride frost sorbents. It is apparent that these frosts have pumping speeds comparable to carbon dioxide but also have somewhat lower saturation capacities.

5.2 ANALYSIS OF INITIAL PUMPING SPEED

The initial hydrogen pumping speed of various frost cryosorbents has been shown to be independent of the volume of the frost, but it is altered as the structure of the frost is changed. Thus, while sorption capacity of the frost is primarily governed by the bulk structure of the frost, the initial pumping speed depends upon the surface characteristics of the frost.

The initial pumping speed is primarily governed by the strength of the sorbate-sorbent interaction and their respective temperatures. Gas-surface interactions are very complex, even if the surface is a simple, completely defined crystal structure and the gas is monatomic, because the impinging particle interacts simultaneously with many surface atoms and they in turn interact with subsurface atoms. The cryodeposited sorbents examined in this investigation were intentionally formed in a manner to make them amorphous and disordered. Their surfaces are clearly far from being crystalline. Moreover, these sorbent surfaces depend upon the conditions at which the frost is formed and its temperature history. As a result, the undefined and irregular nature of the frost sorbent surface coupled with diatomic sorbate molecules makes a detailed analytical analysis of the sorbate-sorbent interaction by existing methods impossible. Although some tests have been conducted in scattering monatomic gases from cryodeposits (Ref. 28), the unknown nature of the surface remains as one obstacle to understanding and predicting the gas-cryofrost interaction process.

The interaction potential of a gas-surface combination is greatly complicated by the fact that a gas particle interacts simultaneously with a great many atoms or molecules in the surface (Fig. 17). Stickney (Ref. 12) has illustrated the complexity of specifying a gas-surface interaction potential function by the highly idealized sketch given in Fig. 17. Because it is under the attractive influence of several surface atoms, a particle which becomes adsorbed in a "valley site" is subject to different forces and is more strongly bound to the surface (i.e., is in a deeper potential well) than is one on a "hill site." It is apparent that a "valley site" is a more probable location for an adsorbed particle to reside. Also, the existence of adsorbed gases still further complicates the problem, because the incident particle may interact with atoms or molecules already adsorbed on the surface. As a result it is only possible to consider the functional form of the interaction potential in a highly approximate way. The Lennard-Jones (6-12) or Morse potential functions were initially proposed to mathematically represent the gas-gas interaction, and for convenience are often used to approximate gas-surface interactions (for example, see Refs. 29 to 31). The Lennard-Jones (6-12) function is expressed,

$$V(r) = 4\epsilon\left[\left(\frac{\sigma}{r}\right)^{12} - \left(\frac{\sigma}{r}\right)^{6}\right]$$

where ϵ represents the depth of the potential well.

The experimental results demonstrate that the pumping speed depends, in part, on the nature of the sorbent surface. Further, the preceding discussion suggests that it is the gas-surface interaction which initially governs the pumping process. It is clear from Eq.

(6) that the pumping speed can be increased if the desorption energy and/or capture probability are increased. Both of these factors may be made larger by increasing the depth of the sorbate-sorbent interaction potential well. Since adsorbed molecules must gain enough energy to get out of the potential well, the desorption energy is about equal to the well depth. If the well is deep, E_d is large and adsorbed molecules are not readily desorbed. A large attractive potential also enhances the chances of adsorption and hence increases the capture probability. Consequently, the potential well depth should be an index indicating the relative pumping speeds of various kinds of sorbents.

Since pumping speeds have been measured for several sorbent species both here and by other investigators, an attempt has been made to correlate initial pumping speeds with the depths of interaction potential wells. Because of the extremely complex nature of the interaction, as briefly outlined above, the actual potential functions and well depths are unfortunately not known. Consequently, they have been grossly approximated by considering the interaction between a sorbate molecule and a single unconfined molecule in the sorbent. Well depth energies for the Lennard-Jones (6-12) potential function are available for a wide variety of gases and were utilized for this purpose. Since this highly simplified sorbate-sorbent interaction is still between different molecular species, the effective interaction potential well depth parameter was taken as

$$\frac{\epsilon_{j,k}}{k} = \sqrt{\left(\frac{\epsilon_j}{k}\right)\left(\frac{\epsilon_k}{k}\right)}$$

The effective well depths of hydrogen sorbate interacting with various sorbents are given in Table I (Appendix III).

Hunt, et al. (Ref. 2) have investigated the largest variety of frost sorbents, but their initial pumping speed data are somewhat irregular as shown in Fig. 1. As a result, estimates of the initial pumping speeds for those tests were obtained from faired extrapolations of the Fig. 1 curves. Initial pumping speed data from the present investigation on the other hand are quite regular (Figs. 11 to 16). All of the available initial pumping speed data obtained with different sorbents are summarized in Fig. 18, and are observed to be reasonably well correlated by the interaction well depth parameter. Although the correlation parameter, $\epsilon_{j,k}/k$ for a simple Lennard-Jones molecule-molecule interaction is highly approximate, it apparently can be used to classify at least roughly the pumping speed potential of prospective frost cryosorbents. The classification criterion is that if the sorbent is to have a high initial pumping speed it should interact strongly with the sorbate molecules and $\epsilon_{j,k}$ should be large.

Other observed phenomena may also be explained in terms of the interaction potential well. A decrease of the hydrogen pumping speed of a carbon dioxide frost when nitrogen was introduced into the system has been noted by Dawbarn (Ref. 4) and by Yuferov and Busol (Ref. 5). This effect, in part, may be due to weakening the sorbate-sorbent interaction. The effective well depth of a hydrogen-carbon dioxide interaction characterized by a value of $\epsilon_{H_2,CO_2}/k = 79.5°K$. If nitrogen is present, it is cryopumped forming a film on the existing carbon dioxide frost surface and the hydrogen molecules now interact with a solid nitrogen surface. Since the interaction

potential of hydrogen with nitrogen is $\epsilon_{H_2,N_2}/k = 55.2°K$, the presence of nitrogen reduces the well depth. Decreasing the adsorptive well depth decreases the pumping speed as shown by Eq. (6).

Equation (6) also shows how the frost temperature influences the initial pumping speed. If the frost temperature is decreased, the desorption term (second term on right-hand side) decreases and the initial pumping speed increases. In addition, decreasing T_f is conducive to increasing the sticking probability, c, although the functional dependence is not known. The variation of S with T_f indicated by Eq. (6) is also observed with the present experimental data (Fig. 13) and the results published by Dawbarn (Ref. 4) and by Yuferov and Busol (Ref. 5).

Frosts which were formed in a manner to make them more disordered, thus giving them more irregular surfaces, exhibited higher capacities but had slightly lower initial pumping speeds (Fig. 14). In contrast, warming and recooling the frost promotes a more ordered and smoother surface and increases initial pumping speed (Fig. 15). These two effects are consistent and suggest that frost cryosorbents with smoother surfaces will have higher initial pumping speeds. This may occur because a smoother frost surface may (1) result in a stronger total interaction with the sorbate molecules and/or (2) result in conditions which decrease the flux of desorbed molecules. It also suggests that surface effects may be limiting the pumping speeds of the much more porous frosts.

5.3 COMPARISON OF SORPTION THEORY WITH EXPERIMENT

Inspection of Fig. 6 reveals that for short times the limit of Eq. (32) is

$$J_o = n_o(D_1/\ell_1)$$

which in terms of the initial pumping speed may be written

$$S_o = J_o \frac{kT_g}{P} = n_o\left(\frac{D_1}{\ell_1}\right) \frac{kT_g}{P} \tag{43}$$

While for long times, as saturation is approached, the limit of Eq. (33) is

$$n^* \Big]_{sat} = n_o$$

or in terms of the measured equilibrium capacity,

$$n_o = \frac{(C_{sat})\,(Q_{sorbent})}{V_f\, k\, T_g} \tag{44}$$

Consequently, measured values of the initial pumping speed and equilibrium sorption capacity may be used to determine n_o and (D_1/ℓ_1). As a result, the only remaining undefined factor is the diffusion constant of the bulk solid, D_2. Because there are no known measurements for the diffusion of hydrogen in cryodeposited frost, Eqs. (32) and (33) must be solved with D_2 as an adjustable parameter. The results of such calculations should provide values of the diffusion constant which are consistent with other characteristics of the frost.

Values of n_o and (D_1/ℓ_1) [obtained from Eqs. (43) and (44)] for the dynamic sorption pumping test results presented here and by Hunt, et al. (Ref. 2) are summarized in Table II. Frost densities given in Ref. 10 were employed to estimate the frost thickness and volume.[3] The value of (D_1/ℓ_1) is a measure of the surface-layer resistance of the frost sorption; a low value of (D_1/ℓ_1) implies high surface resistance. Data from Ref. 2 for carbon dioxide sorbents demonstrate that forming the frost at a high strike rate (or high pressures) results in a sorbent with greater surface resistance. Also, higher temperature frosts would appear to have lower surface resistance.

5.3.1 Experimental Data of Hunt, et al. (Ref. 2)

Theoretical predictions from Eqs. (32) and (33) are compared to experimental results for various sorbents (Ref. 2 data) in Fig. 19. The theoretical curves shown correspond to values of D_2 which appear to best fit the experimental data. The values of D_2 suggested by this comparison are summarized in Table III. This comparison between the experiment and theory illustrates that the simplified two-layer diffusion model is capable of reproducing the variety of dynamic pumping speed curve shapes which have been experimentally observed by Hunt, et al. These investigators formed their frost sorbents very slowly (see Ref. 10), and as a result these frosts were probably the most compact frost cryosorbent ever investigated. Because they are more likely to be diffusion-limited, the proposed theory should compare best with these experimental data.

The information given in Table III illustrates that the sorbent species which have the higher values of the apparent diffusion constant are also characterized by having larger values of the Lennard-Jones well-depth position distance, σ. The parameter, σ, may be grossly interpreted as an index of the structural characteristic of the frost. More compact frosts would be characterized by lower values of σ and, hence, would also be expected to have lower diffusion constants. It should be emphasized that the apparent diffusion constants may only be indicative of the diffusion process in sorbent frosts formed at the conditions of that investigation.

Of the frost sorbents for which data are available, water frost is characterized by the highest diffusion Biot number ($N_D \cong 50$), and, hence, it appears to be the most compact and to have the lowest diffusion constant. The comparison between the experiment and theory implies that internal diffusion dominates the sorption dynamics of water cryosorbents. Carbon dioxide frost, on the other hand, is characterized by a low diffusion Biot number ($N_D \cong 10^{-2}$) for the conditions of the Ref. 2 investigation; consequently, carbon dioxide frost would have a much higher diffusion constant. In this case the ability of the adsorbed molecules to penetrate into the carbon dioxide frost appears to determine its sorption dynamics.

---

[3]Calculations were not made for the N_2O sorbent investigated in Ref. 2 because the front density was not known.

5.3.2 Experimental Data of This Investigation

Some of the pumping speed curves from this investigation for the sorption of hydrogen by carbon dioxide frost as well as the carbon dioxide frost data of Ref. 2 are compared with theoretical calculations in Fig. 20. It is observed that the theoretical calculations with $N_D = 10^{-4}$ agree reasonably well with the present experimental data for frost formed at the lowest strike rate employed, $\dot{n} = 6.3 \times 10^{14}$ molecules/cm^2-sec. Generally, the more ordered and compact carbon dioxide frosts formed at low strike rates have dynamic pumping curves which can be duplicated by the simplified two-layer, diffusion-limited solution (Figs. 20a and b). However, carbon dioxide frosts formed at higher strike rates and, hence, made more porous, exhibited pumping speeds which decreased much more abruptly than this model could predict (Figs. 20c and d). It is believed that these more porous frosts have such high values of the diffusion constant that neither diffusion away from the surface nor in the interior of the frost is the rate-limiting process. As a result the two-layer diffusion model is not applicable. The sorption characteristics of these more porous frosts are believed to reflect the fact that they are adsorption-rate limited.

5.3.3 Summary of Application of Theory

Although a completely general sorption theory has not been derived because of the complex boundary condition at the frost, comparison of experimental results with simplified theories indicated that frost cryosorption may be controlled by (1) adsorption rate, (2) surface penetration, and (3) the internal diffusion rate. The structural characteristics of the frost determines which mechanisms are dominant.

If the frost is formed in a manner to make it more compact, then diffusion appears to govern its sorption behavior. An approximate solution obtained for the special case of surface-penetration and diffusion-dominated sorption [Eqs. (32) and (33)] produced results that agreed with the experimental sorption characteristic of the more compact frosts which would be expected to be diffusion limited.

On the other hand, if the frost sorbent is formed at a rapid rate and at temperatures well below that needed to cryopump it, it is quite porous and its sorption characteristics are dominated by the rate at which molecules can be adsorbed on the surface. Equations (32) and (33) are apparently not valid for the most disordered and porous frosts formed during this investigation. However, lack of knowledge about the reflection and desorption properties of the sorbate molecules for a wide variety of frost species and frost structures will limit the analysis and formation of adsorption-rate limited sorption.

SECTION VI
CONCLUSIONS

Sorption pumping is basically a dynamic process during which the pumping speed decreases from some initial value and approaches zero as the frost is saturated by the sorbate at some equilibrium condition. As a result of this experimental and analytical

investigation of frost cryosorption pumping, it is now possible to put the various facets of this dynamic pumping process into much clearer perspective.

Initial Pumping Speed

1. It appears that the initial pumping speed (s_0) is primarily governed by the nature of the sorbent surface and the gas-surface interaction between the sorbate and the frost sorbent. Equation (6) summarizes the various factors which govern the initial pumping speed. Its use, however, is limited, and accurate prediction of s_0 requires a much better understanding of the sticking probability and desorption characteristics of the sorbate-sorbent system than is currently available.

2. Although only limited data are available, a sorbent which interacts strongly with the sorbate molecules will exhibit greater initial pumping speeds. The initial pumping speed of a carbon dioxide sorbent for hydrogen can be somewhat increased by forming the frost in a manner to give it a smoother surface. This may be achieved by lowering the strike rate and/or increasing the temperature at which the sorbent is deposited, which apparently changes the interaction phenomena of the sorbate with the sorbent surface.

3. Carbon dioxide frost sorbents which have been investigated the most extensively, have an initial pumping speed of about 30 liters/cm^2-sec; this corresponds to an effective capture probability of about 0.7. Other sorbents exhibit pumping speeds from a few liters/cm^2-sec to about 40 liters/cm^2-sec for water frost.

Sorption Dynamics

1. The dynamic sorption characteristics of frost cryosorbents are governed by one or some combination of the following factors: (a) the rate at which molecules are adsorbed on the surface, (b) the rate at which they are able to enter the interior of the frost, and (c) their diffusion rate into the frost structure.

2. Analysis of a diffusion-limited sorption model has shown that the pumping dynamics of only very compact frost cryosorbents would be governed solely by the diffusion into the frost structure.

3. A more complicated two-layer diffusion model has been proposed. This model assumes that sorbate molecules are adsorbed onto the frost surface, and then they diffuse into the frost which is treated as if it consisted of two layers, each characterized by a different diffusion constant. Thus, according to this theory when the sorption process is not adsorption-rate limited, the sorption dynamics depends upon how well molecules migrate away from the surface and diffuse into the frost.

4. The two-layer diffusion model, as summarized by Eqs. (32) and (33) for the case of an infinitesimal surface layer, can produce theoretical sorption curves which agree with many of the experimentally observed curves for the more compact frosts.

5. Application of the theory implies that water frost at 11°K, for example, is rather compact and has an apparent diffusion constant as low as 10^{-15} cm^2/sec. On the other hand, carbon dioxide frosts are much more amorphous and have apparent diffusion constants between 10^{-8} to 10^{-12} cm^2/sec.

6. Carbon dioxide sorbents which were formed in a manner to make them much more disordered (i.e., at strike rates above about 10^{16} molecules/cm^2-sec) exhibited dynamic sorption curves which decreased much more abruptly than the theory would predict. It is believed that the proposed theory is not applicable to extremely porous frosts and that in this case the pumping process is adsorption-rate limited. This latter case is quite complex and has not yet been analyzed.

7. The diffusion constant for the sorbate in the sorbent is an adjustable parameter in penetration and diffusion limiting solution. Values needed to fit the experimental results for the sorption of hydrogen by carbon dioxide frost were consistent with the rough estimates based on similar systems. Moreover, the diffusion constants varied with frost structure in the expected manner. Since diffusion constants for hydrogen in solidified gases are not available elsewhere, it is suggested that the values given herein may be useful until more definitive and direct measurements can be made.

REFERENCES

1. Brackmann, R. T. and Fite, W. L. "Condensation of Atomic and Molecular Hydrogen at Low Temperatures." Journal of Chemical Physics, Vol. 34, No. 5, May 1961, pp. 1572–1579.

2. Hunt, A. L., Taylor, C. E., and Omohundro, J. E. "Adsorption of Hydrogen on Solidified–Gas Films." Advances in Cryogenic Engineering, Vol. 8, Plenum Press, 1963, pp. 100-109.

3. Southerlan, R. E. "10-20°K Cryosorption of Helium on Molecular Sieve 5A and Hydrogen on Condensed Vapors." AEDC-TR-65-49 (AD463339), May 1965.

4. Dawbarn, Ronald. "Cryosorption of Hydrogen by 12-20°K Carbon Dioxide Cryodeposits." AEDC-TR-67-125 (AD655067), July 1967.

5. Yuferov, V. B. and Busol, F. E. "Sorption of Hydrogen and Neon by Layers of Solids Formed by Vapor Condensation." Soviet Physics–Technical Physics, Vol. 11, No. 11, May 1967, pp. 1518–1524.

6. Müller, E. "Adsorption Isotherms on Solid Carbon Dioxide." Cryogenics, August 1966.

7. Haygood, J. D. and Dawbarn, Ronald. "Helium Pumping by 4.2°K Cryodeposits." AEDC-TR-66-204 (AD645511), January 1967.

8. Dawbarn, Ronald and Haygood, J. D. "Development and Evaluation of a Cryodeposit Sorption Pump Capable of Pumping Helium." AEDC-TR-68-90 (AD675207), September 1968.

9. Yuferov, V. B., Kovalenko, V. A., and Kobzev, P. M. "Helium Sorption by Layers of Condensed Gases." Soviet Physics–Technical Physics, Vol. 12, No. 9, March 1968, pp. 1265–1266.

10. Tempelmeyer, K. E. "Sorption Pumping of Hydrogen by Cryodeposits–Sorption Capacity Measurements." AEDC-TR-69-266 (AD700980), February 1970.

11. Tempelmeyer, K. E. "Sorption Pumping of Hydrogen by Cryodeposits–Prediction of Sorption Capacity." AEDC-TR-69-270 (AD700981), February 1970.

12. Stickney, R. E. "A Discussion of Energy and Momentum Transfer in Gas-Surface Interactions." AEDC-TR-66-13 (AD630522), February 1966.

13. Frenkel, "Adsorption." J. Z. Physik, Vol. 26, No. 2, 1924, pp. 117–138.

14. Heald, J. H., Jr. and Brown, R. F. "Measurements of Condensation and Evaporation of Carbon Dioxide, Nitrogen and Argon at Cryogenic Temperatures Using a Molecular Beam." AEDC-TR-68-110 (AD674596), September 1968.

15. Jost, W. Diffusion in Solids, Liquids, Gases. Academic Press, Inc., Publishers, New York, 1952.

16. Arpaci, Vedat S. Conduction Heat Transfer. Addison-Wesley Publishing Co., Reading Mass. 1966.

17. Ash, R., Barrer, R. M., and Pope, G. G. "Flow of Adsorbable Gases and Vapours in a Microporous Medium." Royal Society of London Proceedings, Series A, Vol. 271, No. 1344, January 1, 1963, pp. 1-18.

18. Onsager, Lars and Runnels, L. K. "Diffusion and Relaxation Phenomena in Ice." The Journal of Chemical Physics, Vol. 50, No. 3, February 1969, pp. 1089–1103.

19. Cremer, E. "Bestimmung der Selbstdiffusion in festem Wasserstoft aus dem Reaktionsverlauf der Ortho-Para-Umwandlung." Zeit J. Physik Chem, Vol. 39B, 1938, pp. 445-464.

20. Carslaw, H. S. and Jaeger, J. C. Conduction of Heat in Solids. Oxford at the Clarendon Press, Second Edition, 1959.

21. Smits, F. M. and R. C. Miller, "Rate Limitation at the Surface for Impurity Diffusion in Semiconductors." Physical Review, Vol. 104, No. 5, December 1956, pp. 1242–1245.

22. Smith, A. M. "Diffusion." Section II, Fundamentals of Silicon Integrated Device Technology, Vol. 1, Prentice-Hall International, London, 1967.

23. Boltaks, B. I. Diffusion in Semiconductors (Translation). Chapter VI, Academic Press, New York, 1963.

24. Hodgman, Charles D., Weast, R. C., and Selby, S. M. Handbook of Chemistry and Physics, Chemical Rubber Publishing Co., 39th Edition, Cleveland, Ohio, 1958.

25. Müller, P. R. "Measurements of Refractive Index, Density, and Reflected Light Distributions for Carbon Dioxide and Water Cryodeposits and also Roughened Glass Surfaces." PhD Dissertation, University of Tennessee, June 1969.

26. Rogers, K. W. "Experimental Investigations of Solid Nitrogen Formed by Cryopumping." NASA CR-553, August 1966.

27. Stewart, J. W. "The Properties of Solidified Gases at High Pressure." Physics of High Pressures and the Condensed Phase (A. van Itterbeck, ed.) Chap. 5, John Wiley and Sons, Inc., New York.

28. Busby, M. R. and Brown, R. F. "Preliminary Investigation of the Interaction of 0.30 to 0.54 ev Gaseous Argon with a Solid Argon Surface." AEDC-TR-69-195 (AD696106), November 1969.

29. Goodman, F. O. "Preliminary Results of a Three-Dimensional Hard-Spheres Theory of Scattering of Gas Atoms from a Solid Surface." Proceedings of the Fifth International Symposium on Rarefied Gas Dynamics, Vol. 1, C. L. Brundin (Ed.), Academic Press, New York, 1967, pp. 35-48.

30. Oman, R. A. "Calculations of the Interactions of Diatomic Molecules with Solid Surfaces." Proceedings of the Fifth International Symposium on Rarefied Gas Dynamics, Vol. 1, C. L. Brundin (Ed.), Academic Press, New York, 1967, pp. 83-100.

31. Ricca, F. "Potential-Energy Profiles in Physisorption on f.c.c. Crystals." Supplements al Nuovo Cimento, Vol. V, 1967, pp. 339–353.

APPENDIXES

I. ILLUSTRATIONS
II. DERIVATION OF EXPRESSIONS FOR PUMPING SPEED AND CAPACITY FOR THE TWO-LAYER DIFFUSION MODEL
III. TABLES

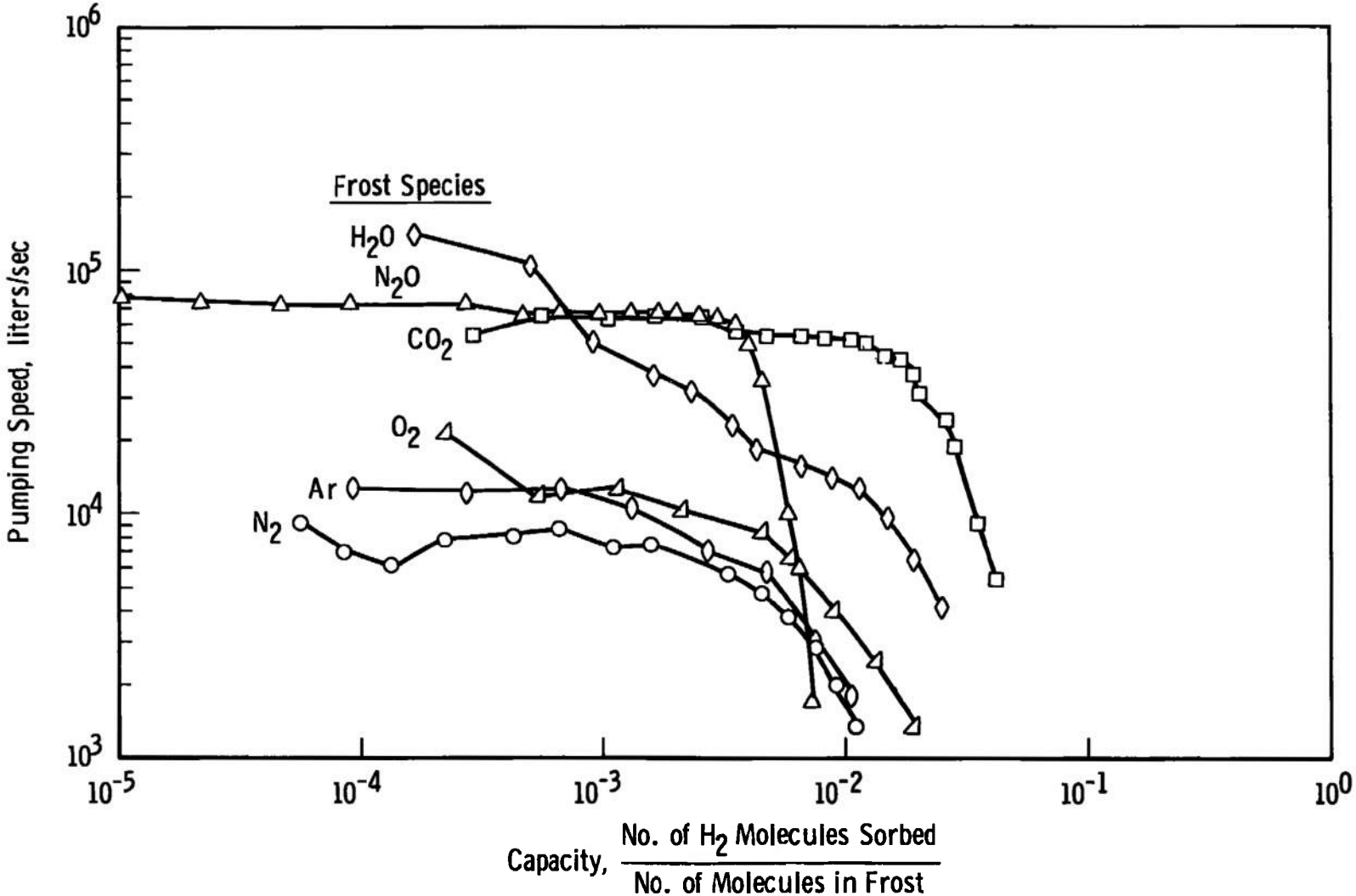

Fig. 1 Dynamic Frost Cryosorption Measurements of Hunt, Taylor, and Omohundro (Ref. 2) for 300°K Hydrogen on Various Frosts at 11°K

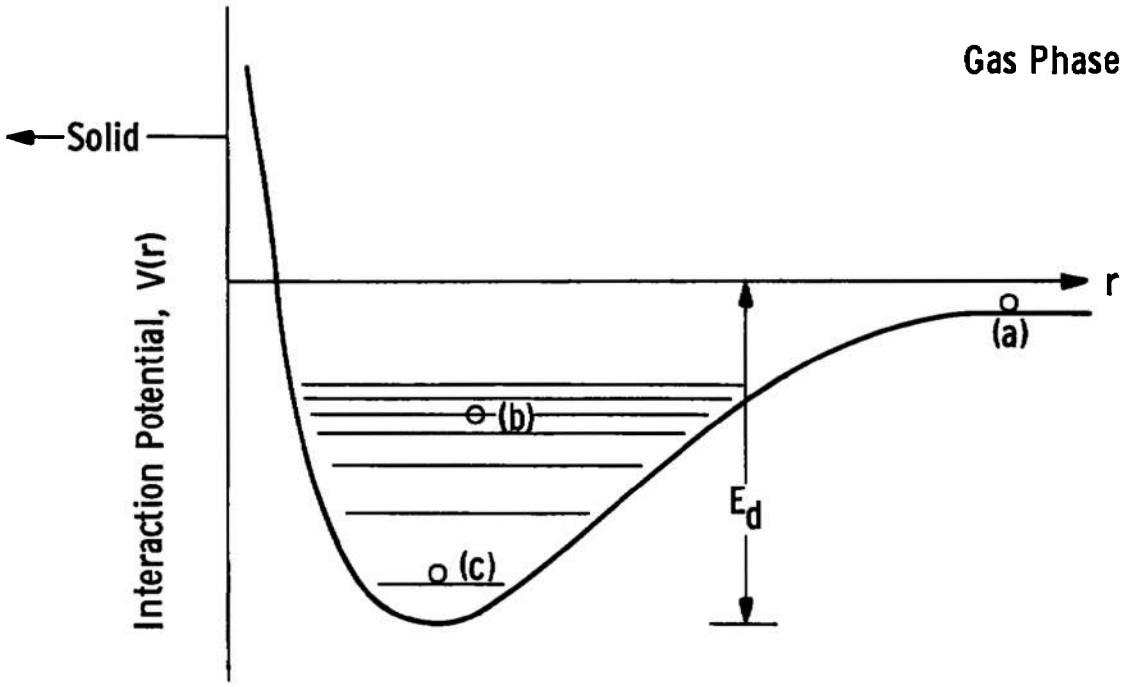

a. Potential Plot for Physical Adsorption

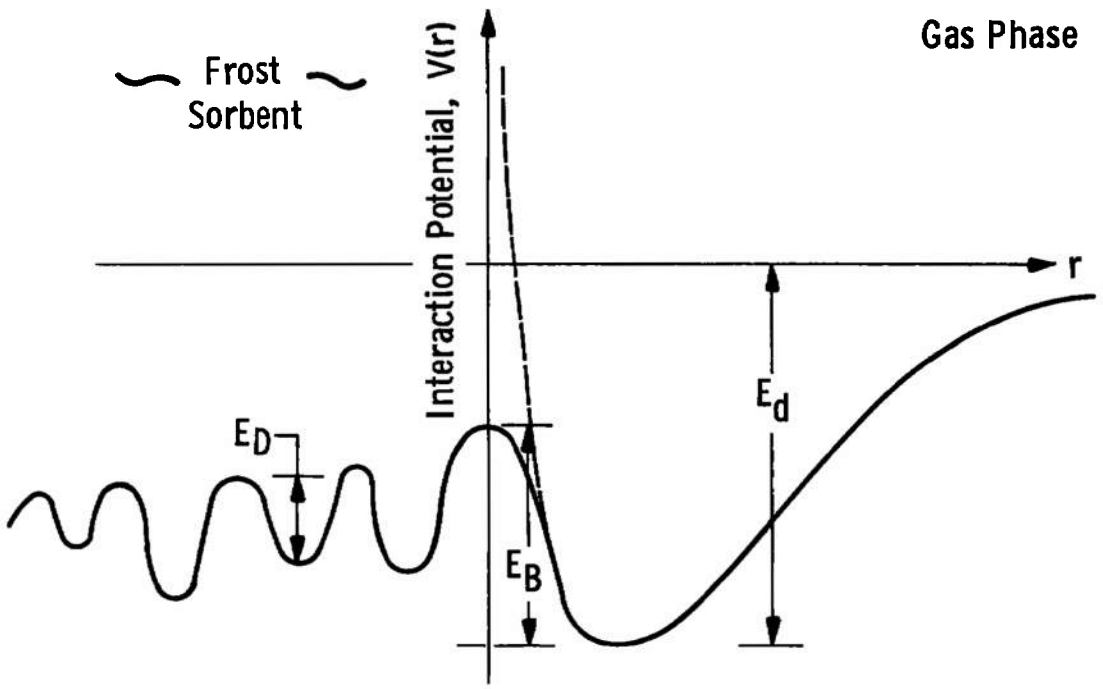

b. Potential Plot for Frost Cryosorption

Fig. 2 Potential Energy Distribution for Physisorption and Frost Cryosorption

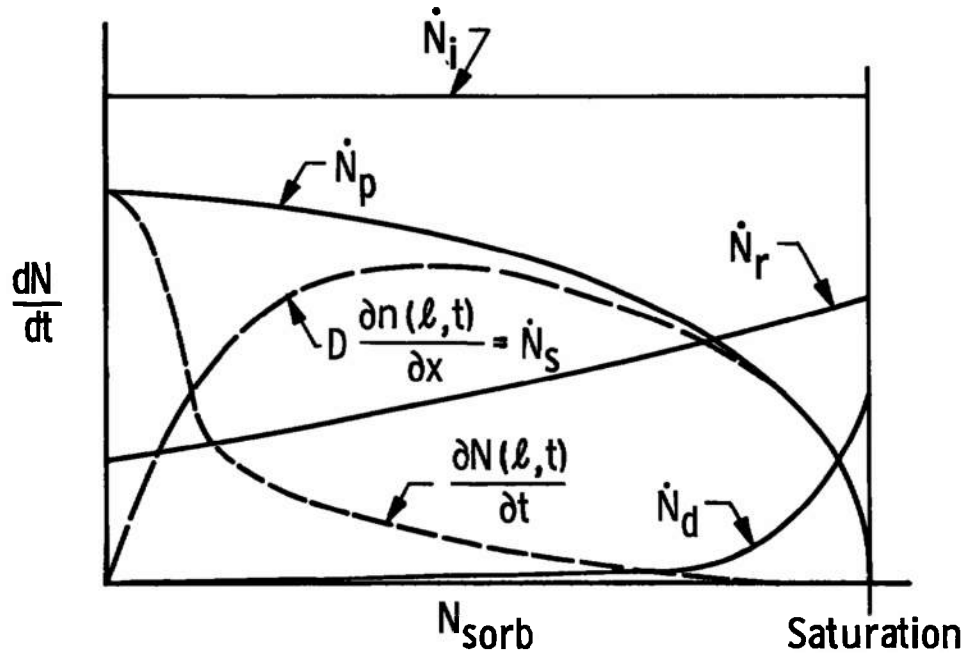

a. General Case

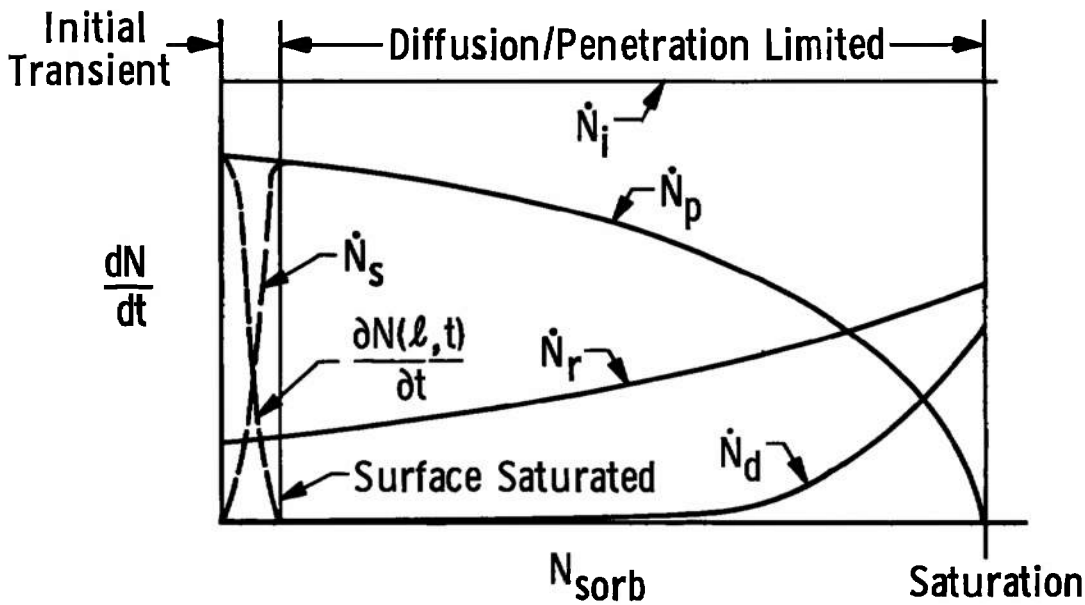

b. Diffusion/Penertration Limited Case

Fig. 3 Schematic of Sorption Dynamics

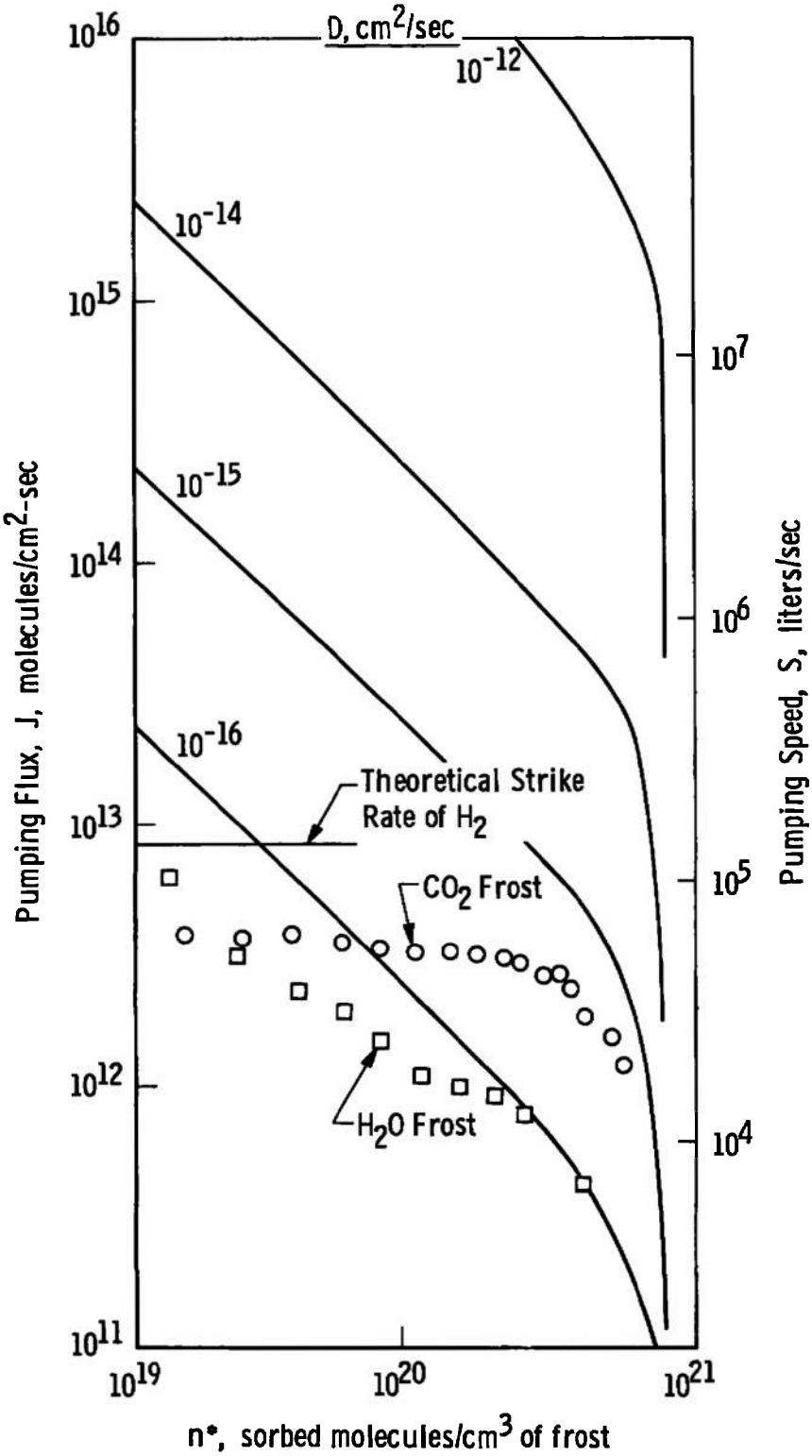

Fig. 4 Comparison of Ref. 2 Data for Water and Carbon Dioxide Frosts with Diffusion-Limited Model

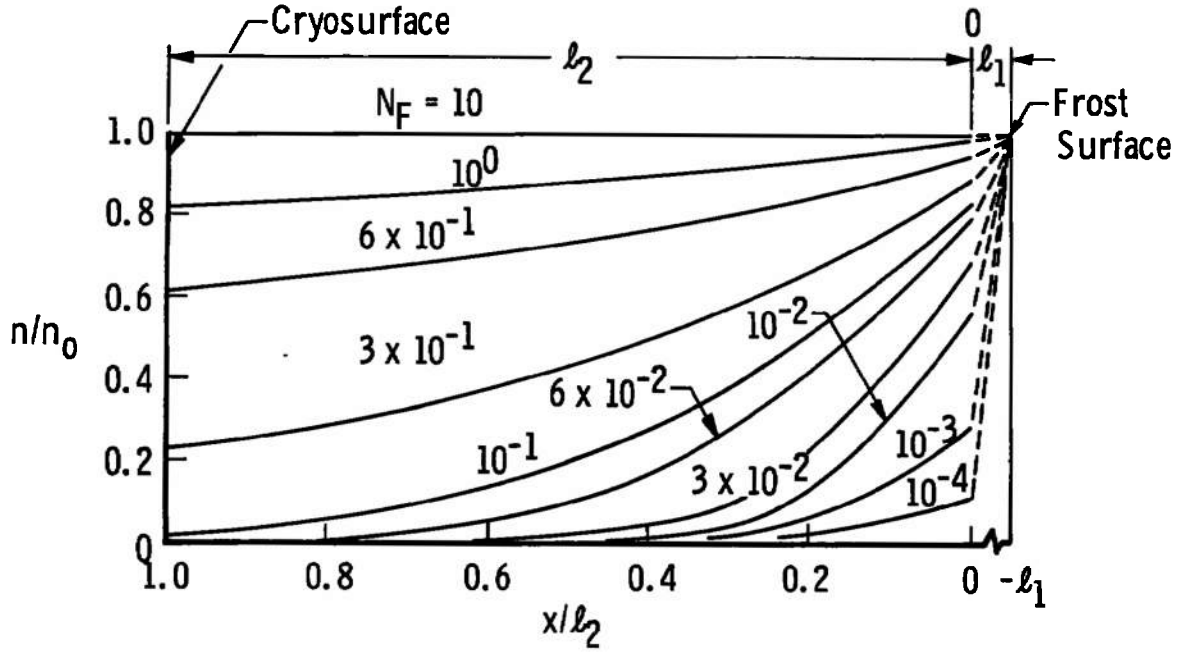

a. $N_D = 10$, $D_2 = 10^{-11}$ cm²/sec

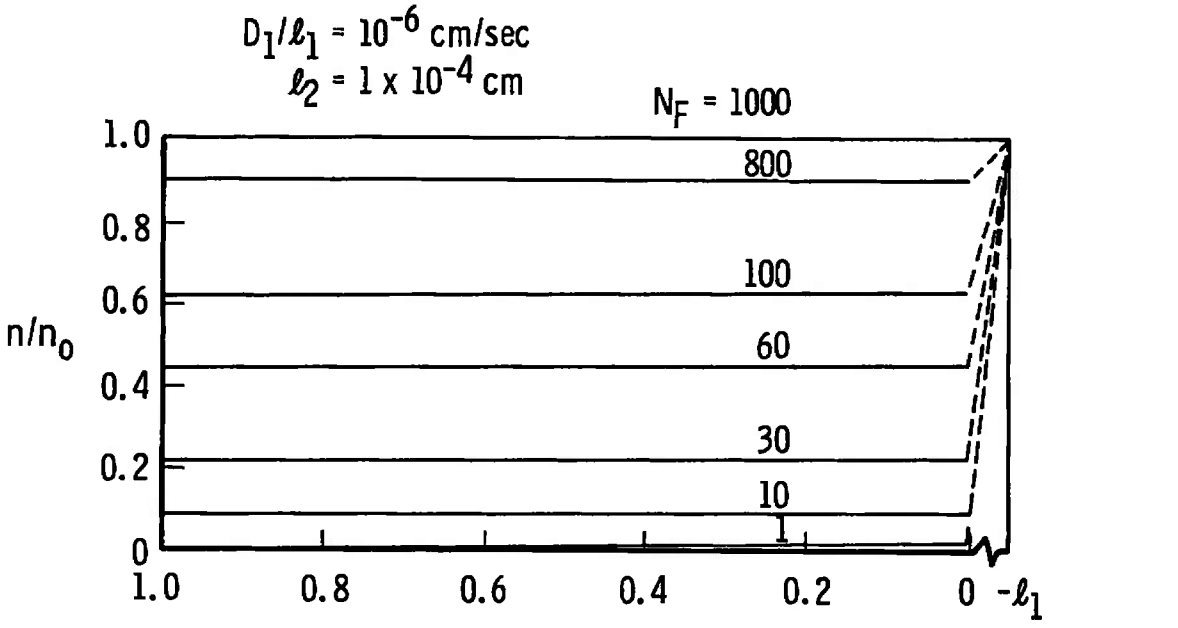

b. $N_D = 10^{-2}$, $D_2 = 10^{-8}$ cm²/sec

Fig. 5 Theoretical Distributions of Sorbate in the Assumed Two-Layer Sorbent Model (Eq. 29)

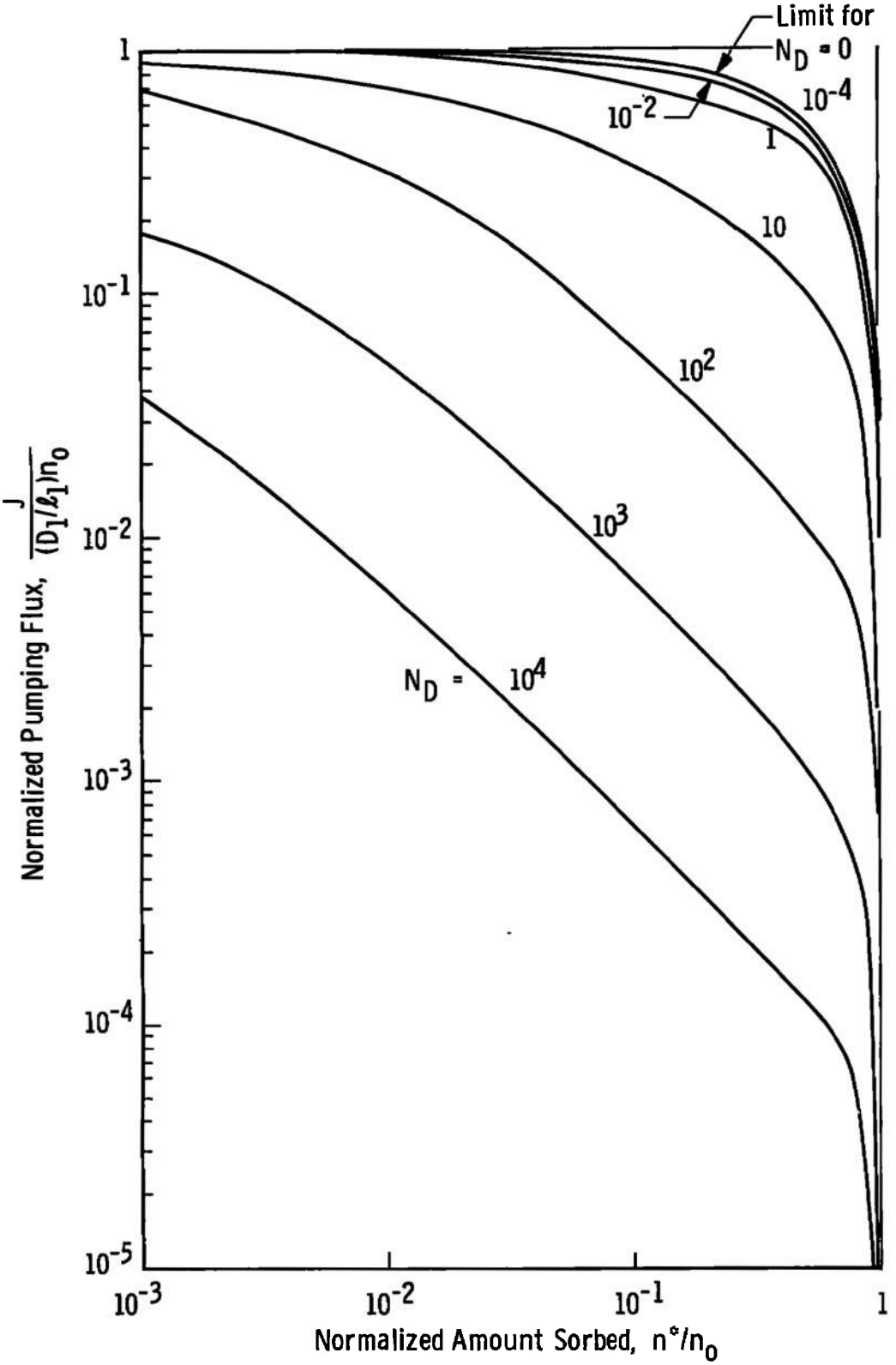

Fig. 6 Theoretical Sorption Pumping Curves Model for the Two-Layer Sorbent

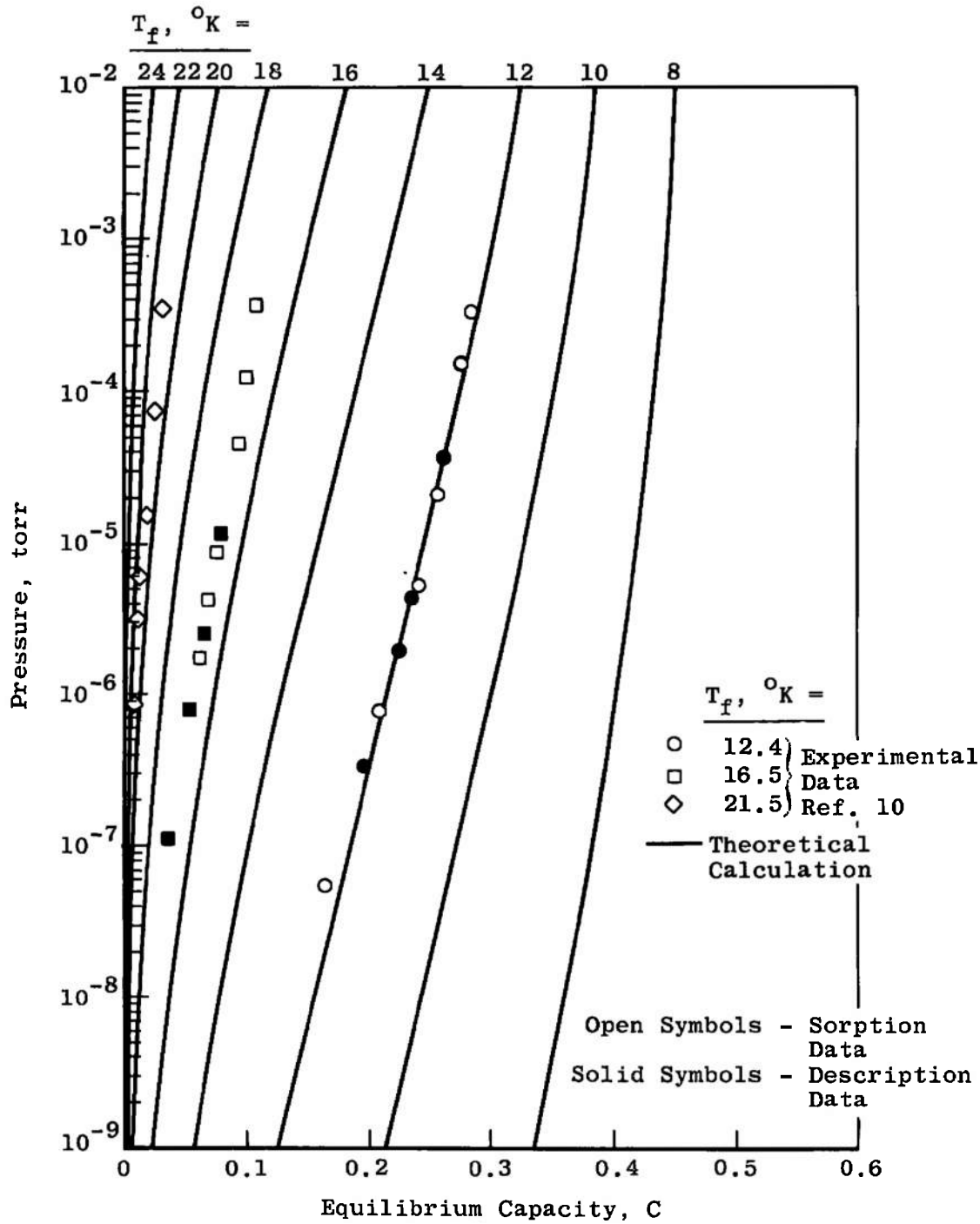

Fig. 7 Comparison of Calculated Hydrogen Equilibrium Isotherms for the Dubinin-Radushkevich Equation for Carbon Dioxide Frost Formed at a Strike Rate of 6.3×10^{15} molecules/cm^2-sec

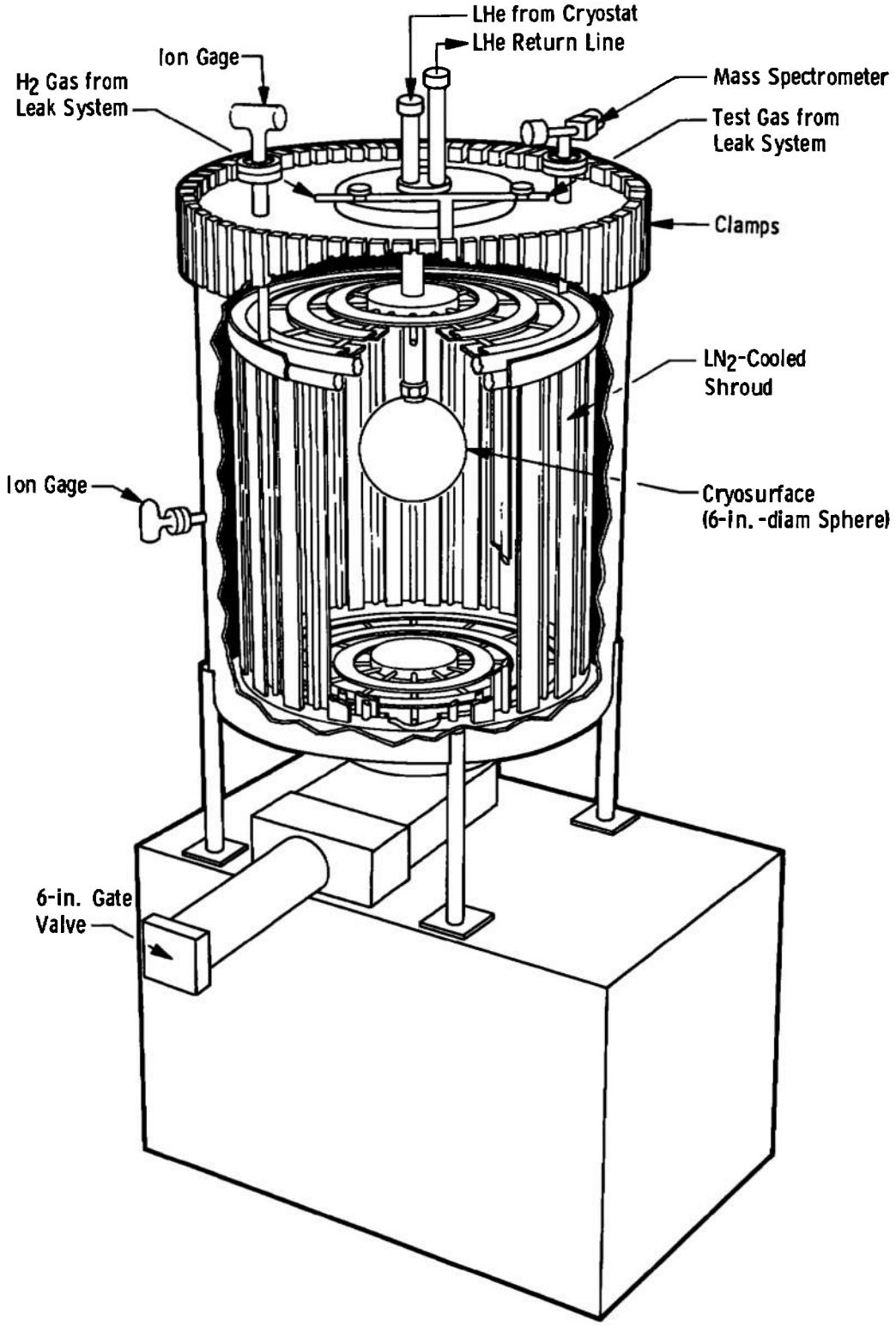

Fig. 8 Schematic of Chamber Used for Hydrogen Cryosorption Tests

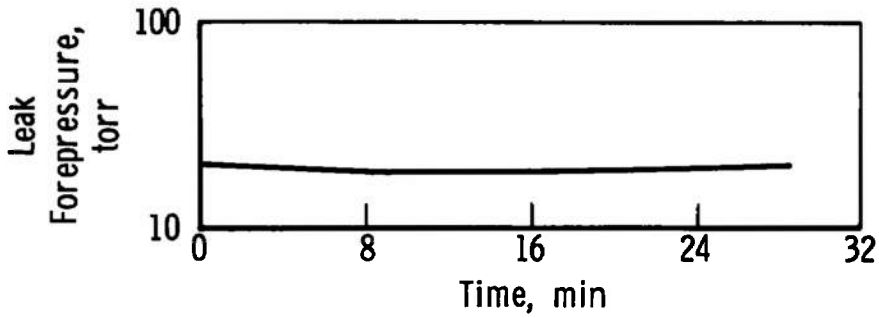

a. Leak Forepressure

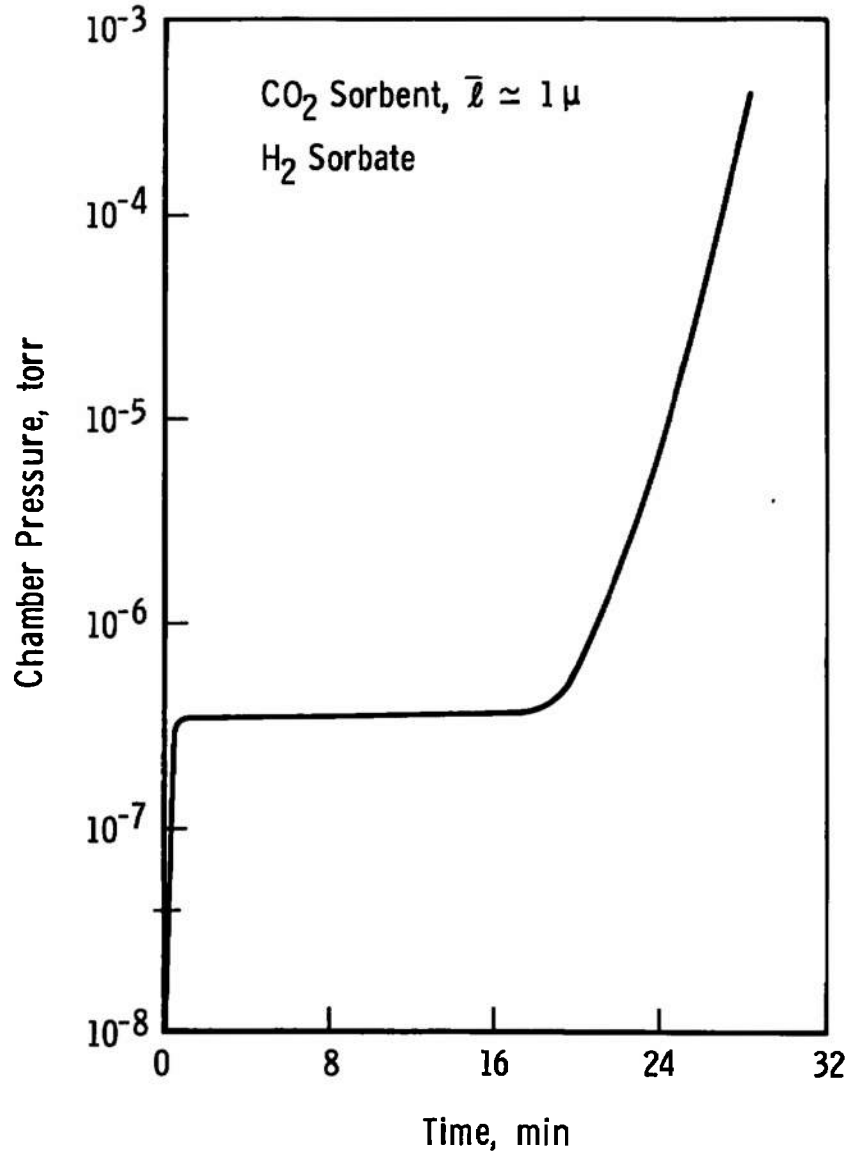

b. Chamber Pressure

Fig. 9 Typical Pressure History for a Test with Constant Sorbate Flow Rate

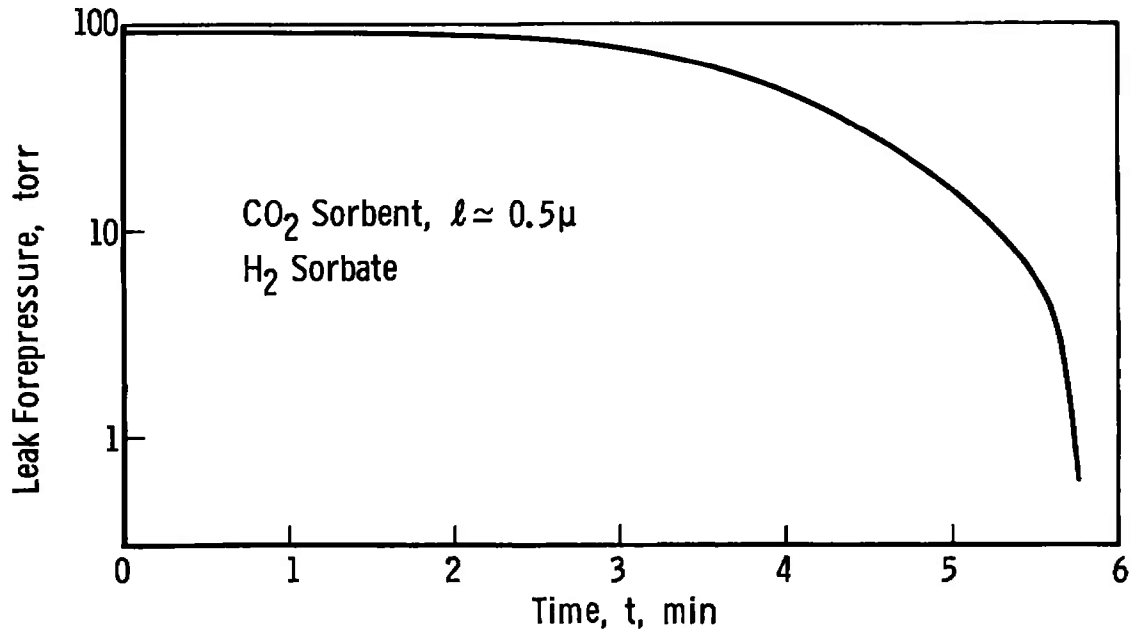

a. Leak Forepressure

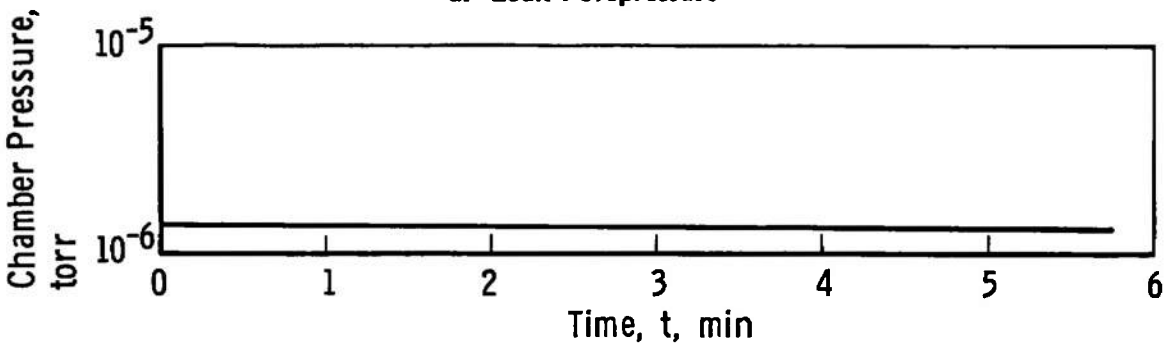

b. Chamber Pressure

Fig. 10 Typical Pressure History for a Test with Variable Sorbate Flow Rate

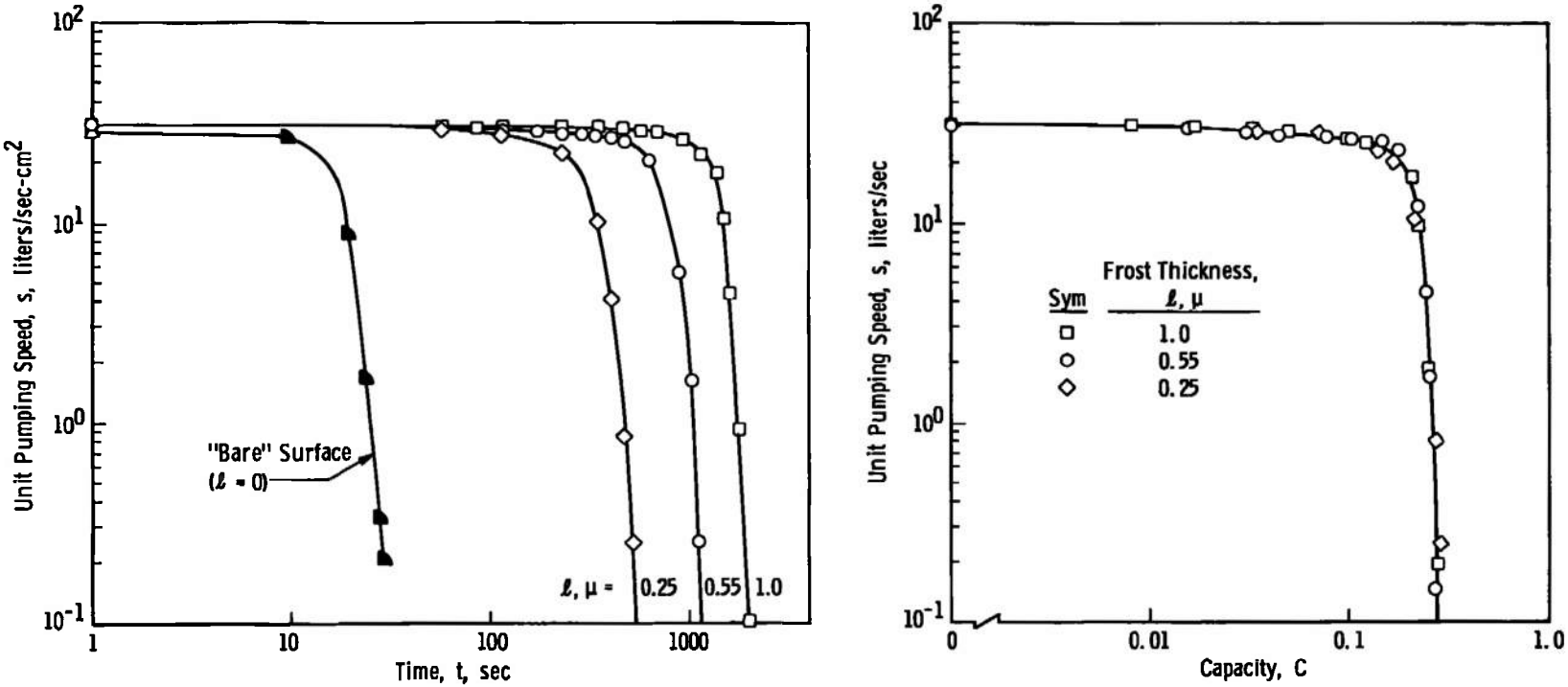

a. Pumping Speed versus Time

b. Pumping Speed versus Capacity

Fig. 11 Dynamic Pumping Speed Curves for Various Thicknesses of 12.4°K Carbon Dioxide Frost Formed at a Chamber Pressure Level of 2×10^{-5} torr on a 12.4°K Surface - Constant Hydrogen Sorbate Addition Rate

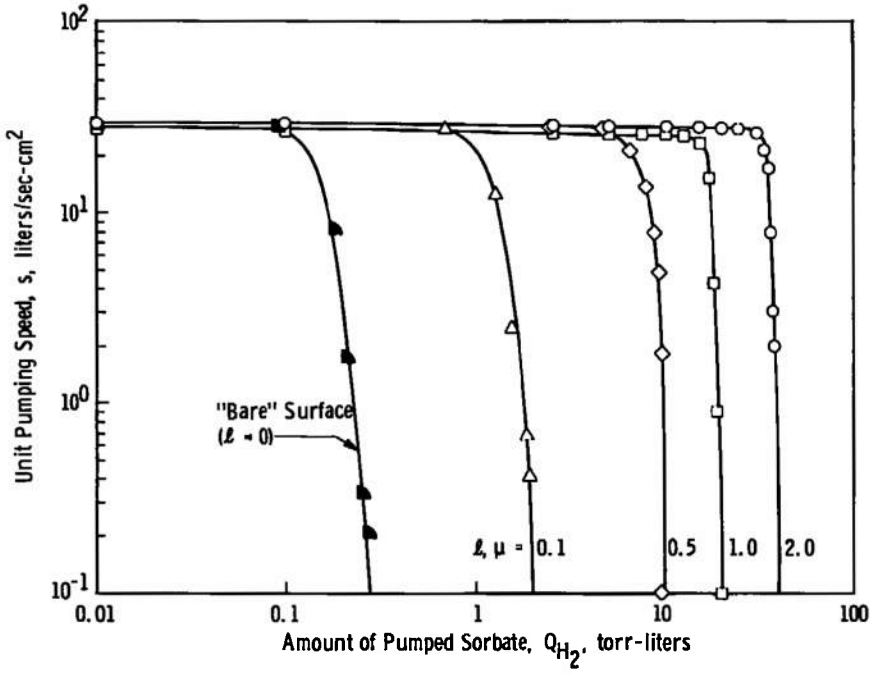

a. Pumping Speed versus Amount of H_2 Sorbed

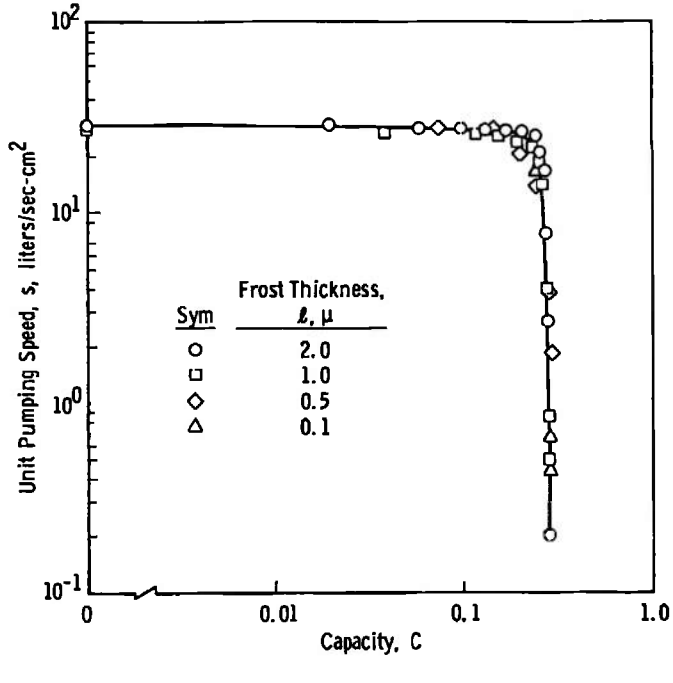

b. Pumping Speed versus Capacity

Fig. 12 Dynamic Pumping Speed Curves for Various Thicknesses of 12.4°K Carbon Dioxide Frost Formed at a Chamber Pressure Level of 2×10^{-5} torr on a 12.4°K Surface - Pumping at Constant Chamber Pressure

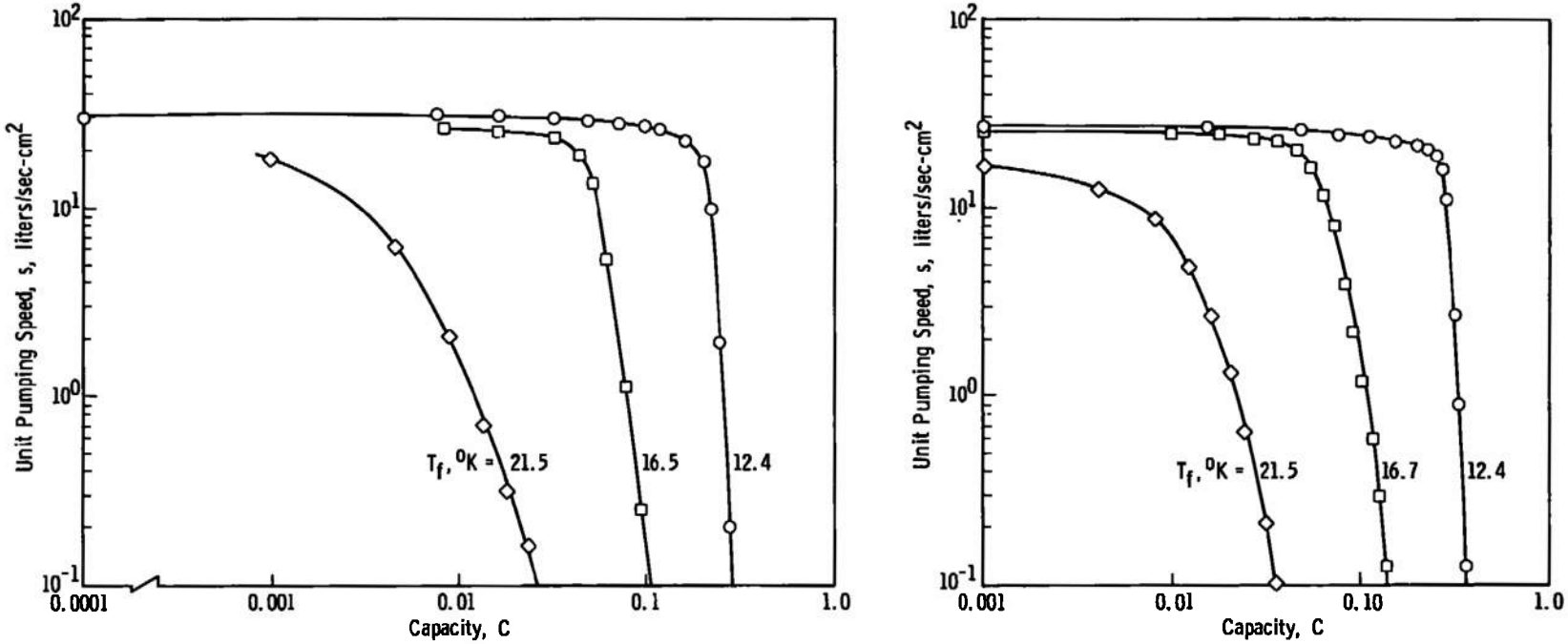

Fig. 13 Dynamic Hydrogen Pumping Speed Curves for Carbon Dioxide Frosts at Various Temperatures - Constant Hydrogen Sorbate Addition Rate

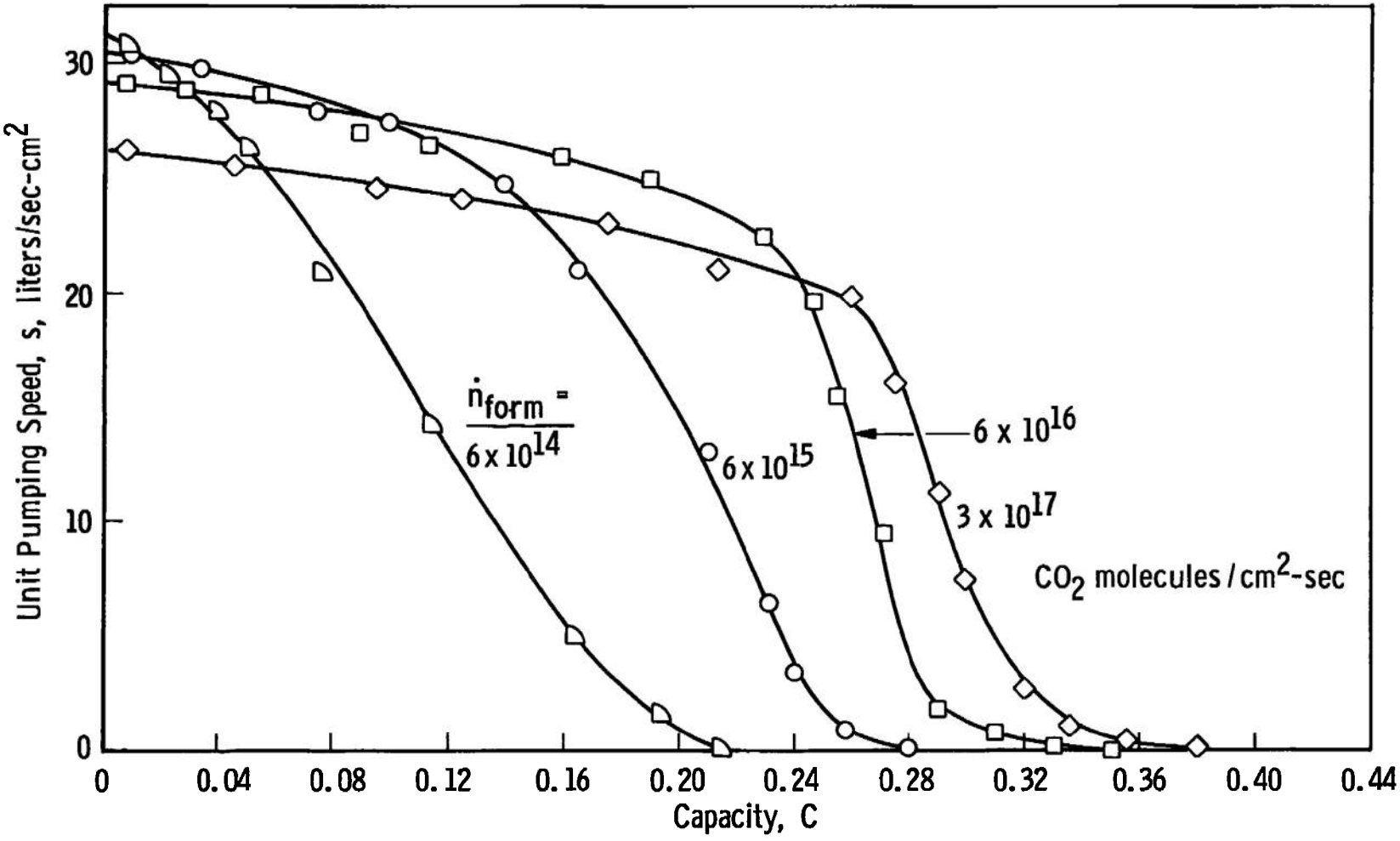

Fig. 14 Dynamic Hydrogen Pumping Speed Curves for 12.4°K Carbon Dioxide Frost Formed at Different Pressure Levels and Strike Rates

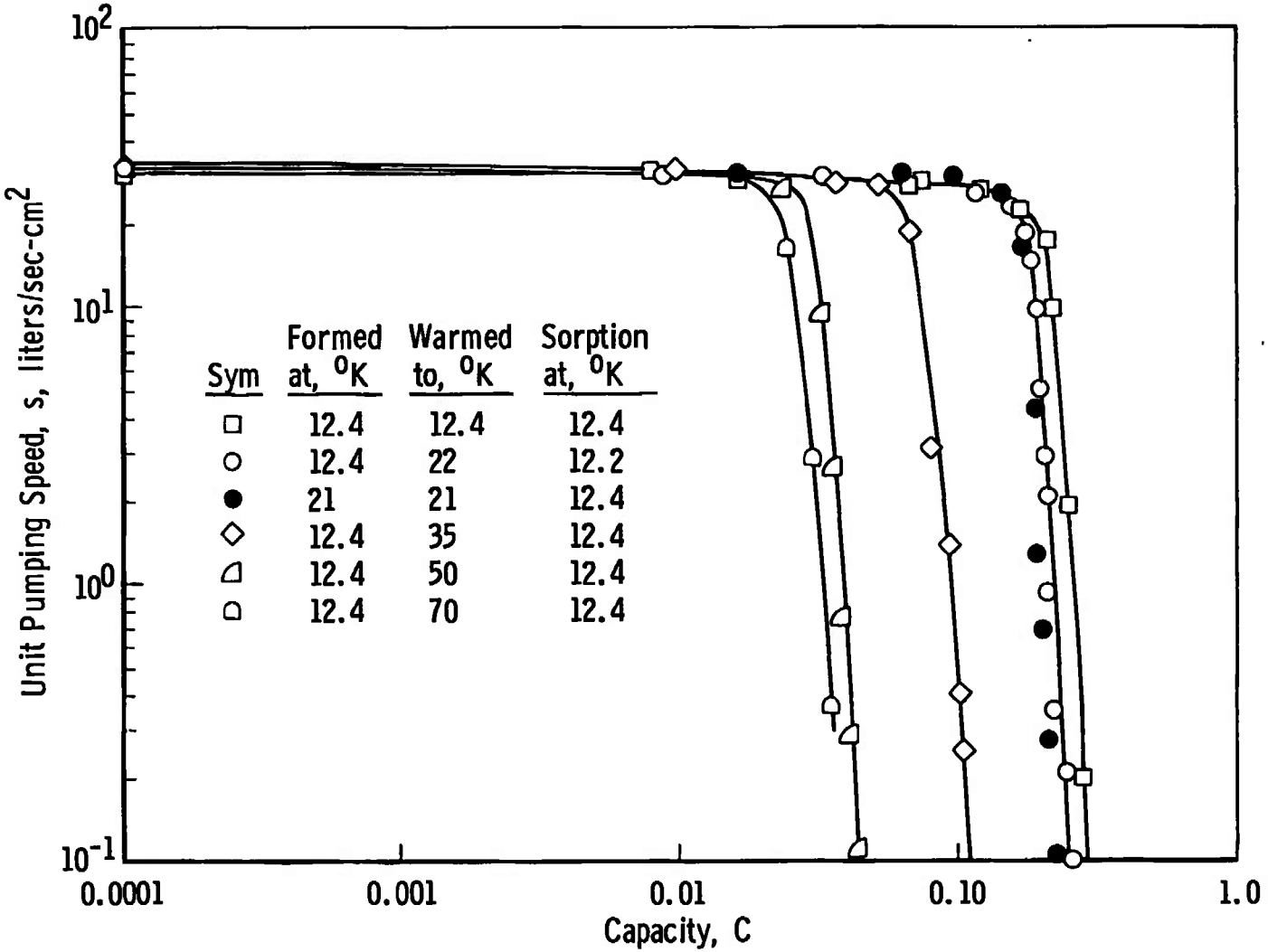

Fig. 15 Dynamic Hydrogen Pumping Speed Curves for Carbon Dioxide Frost Formed at a Strike Rate of 6.3×10^{15} molecules/cm²-sec and a Temperature of 12.4°K but Warmed to Higher Intermediate Temperatures

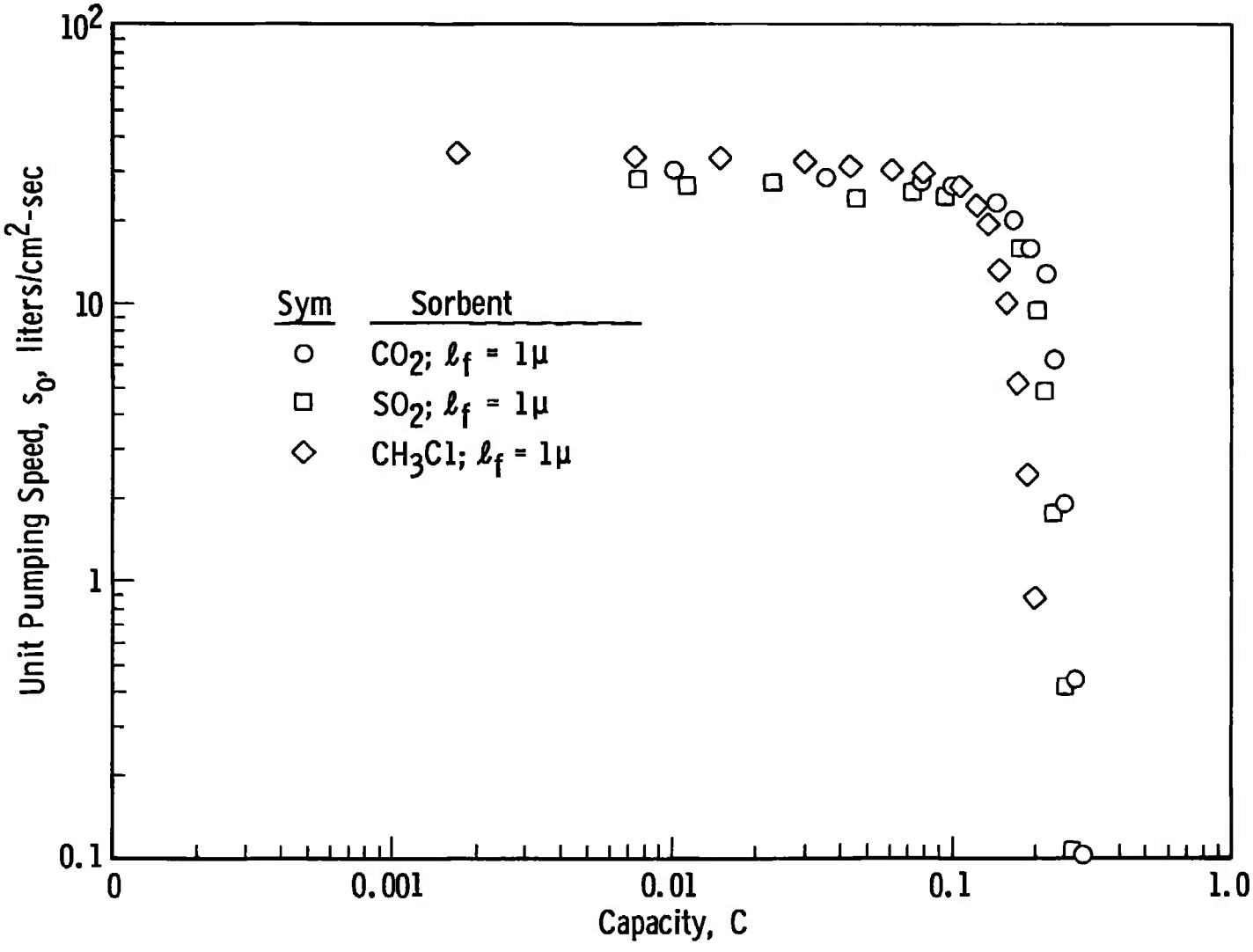

Fig. 16 Dynamic Hydrogen Pumping Curves of Several Sorbents at a Temperature of 12.4°K and Formed at the Same Conditions

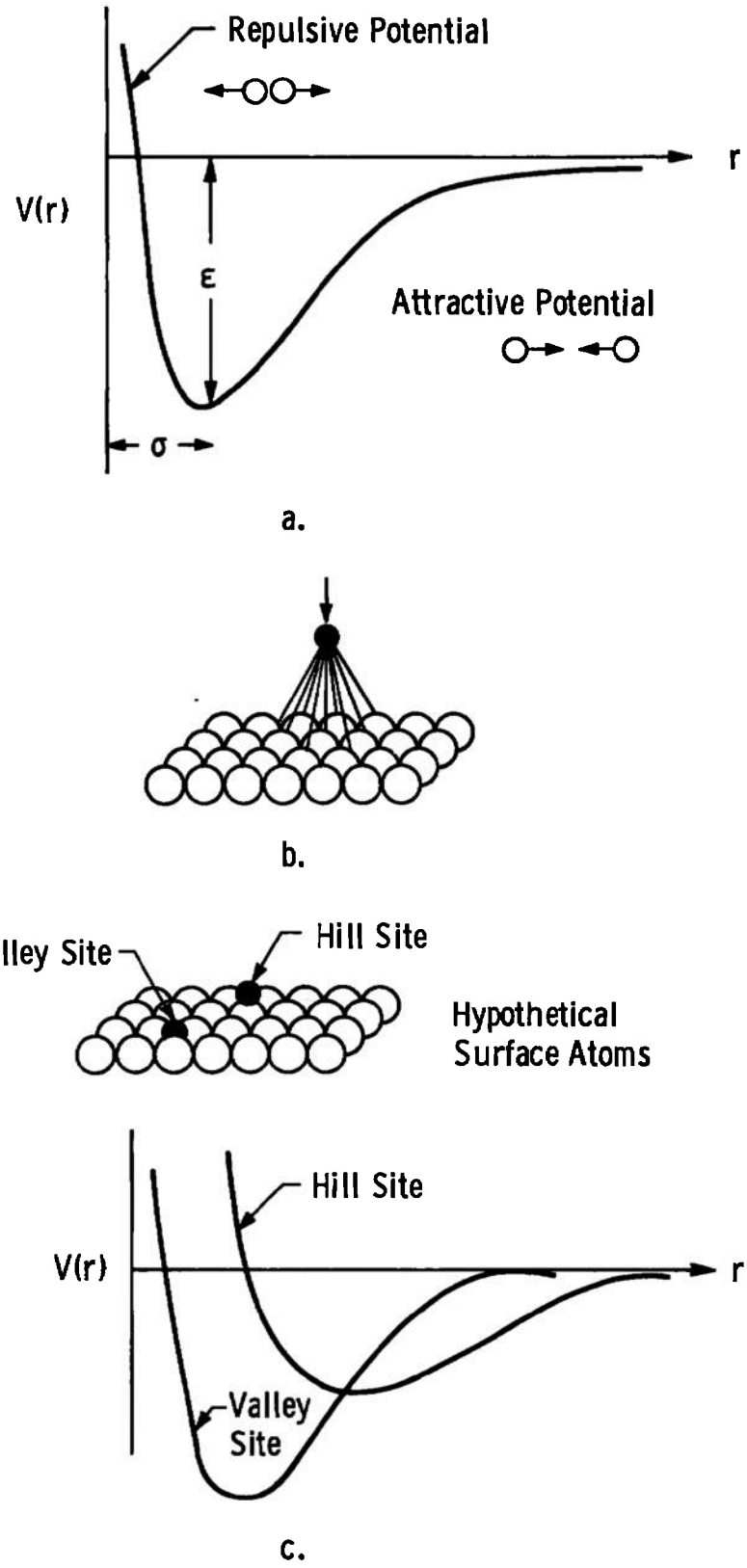

Fig. 17 Simplified Concepts of the Gas-Surface Interaction

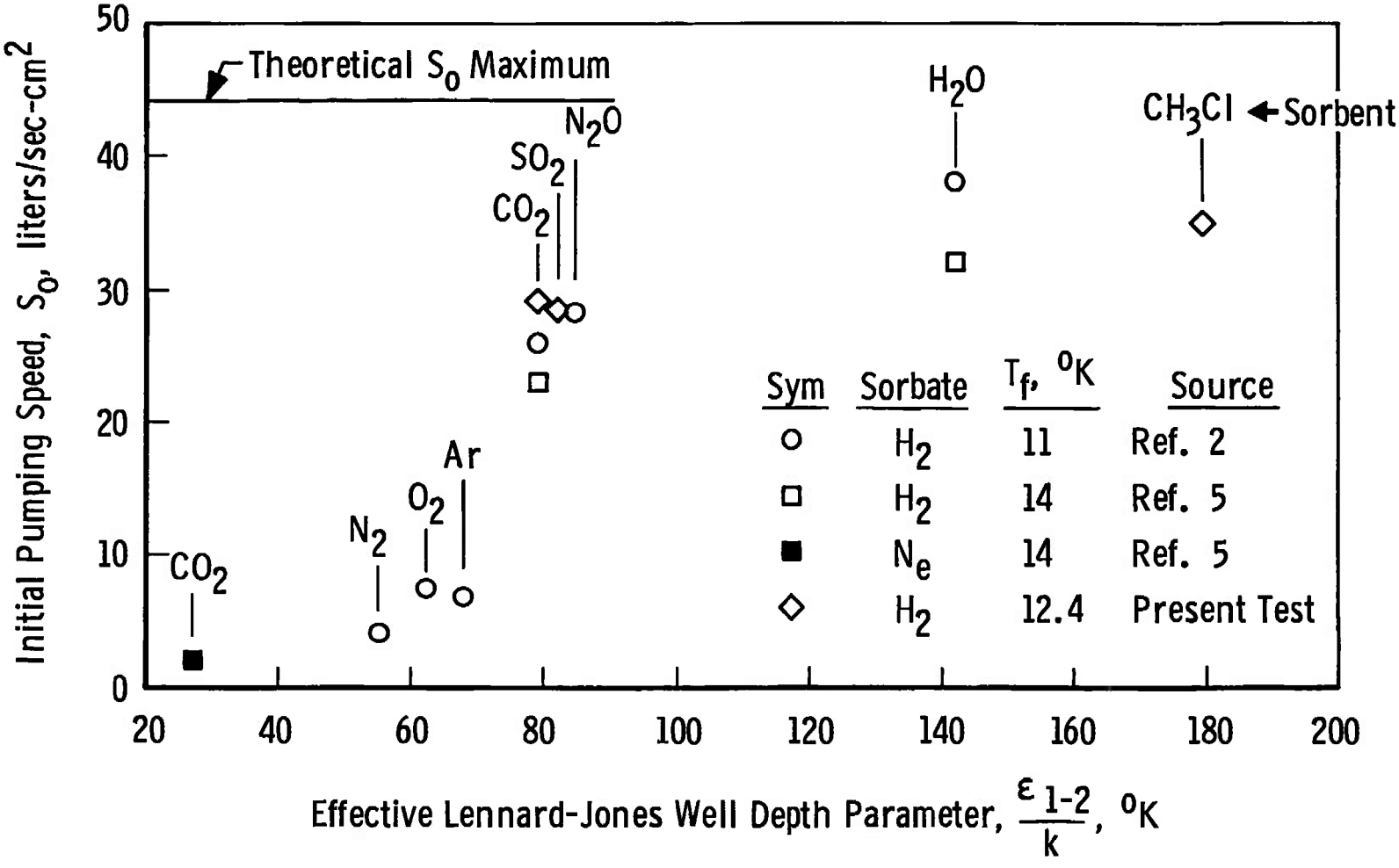

Fig. 18 Correlation of the Initial Sorption Pumping Speeds with the Lennard-Jones Well Depth

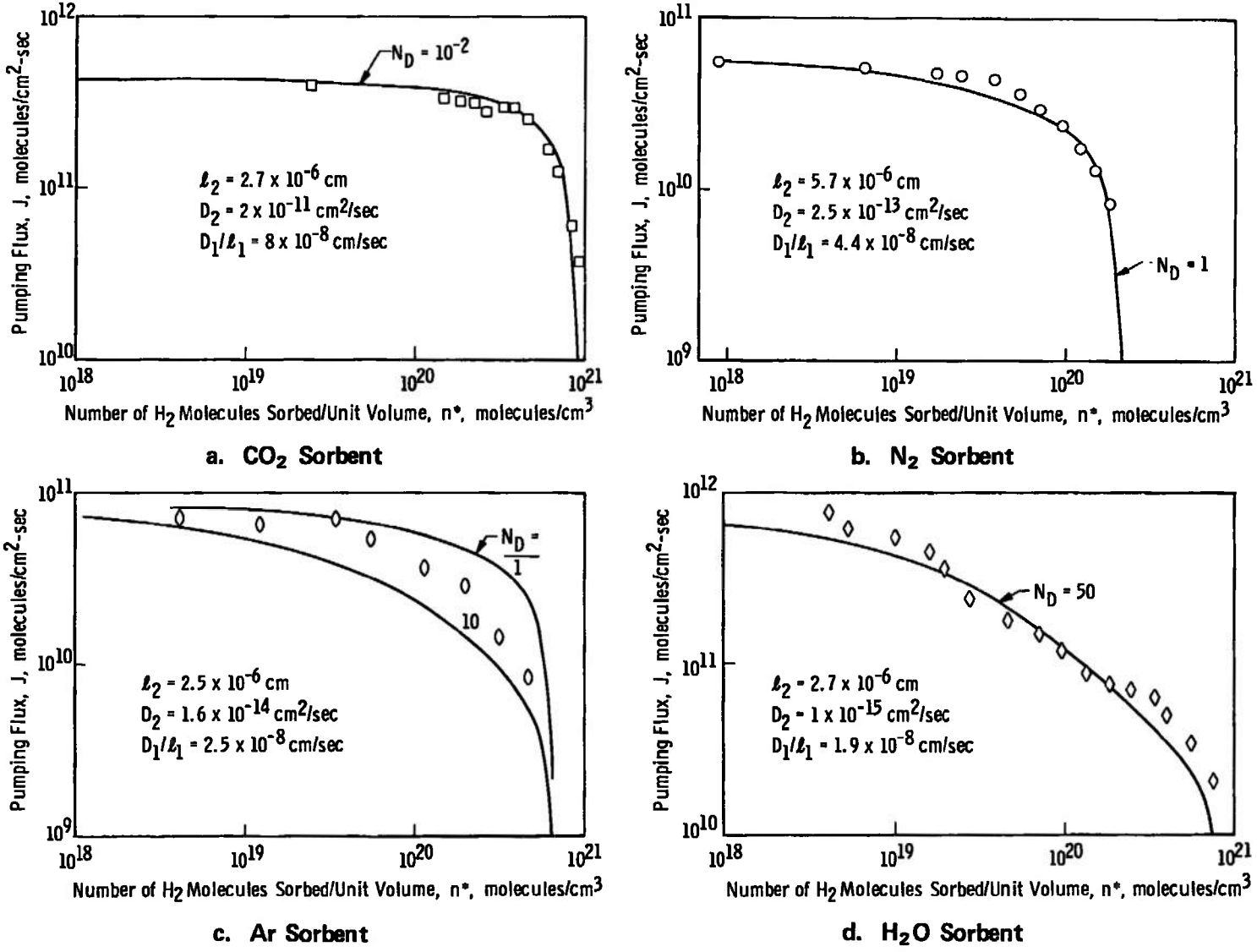

Fig. 19 Comparison of Two-Layer Sorption Theory with Experimental Data of Ref. 2

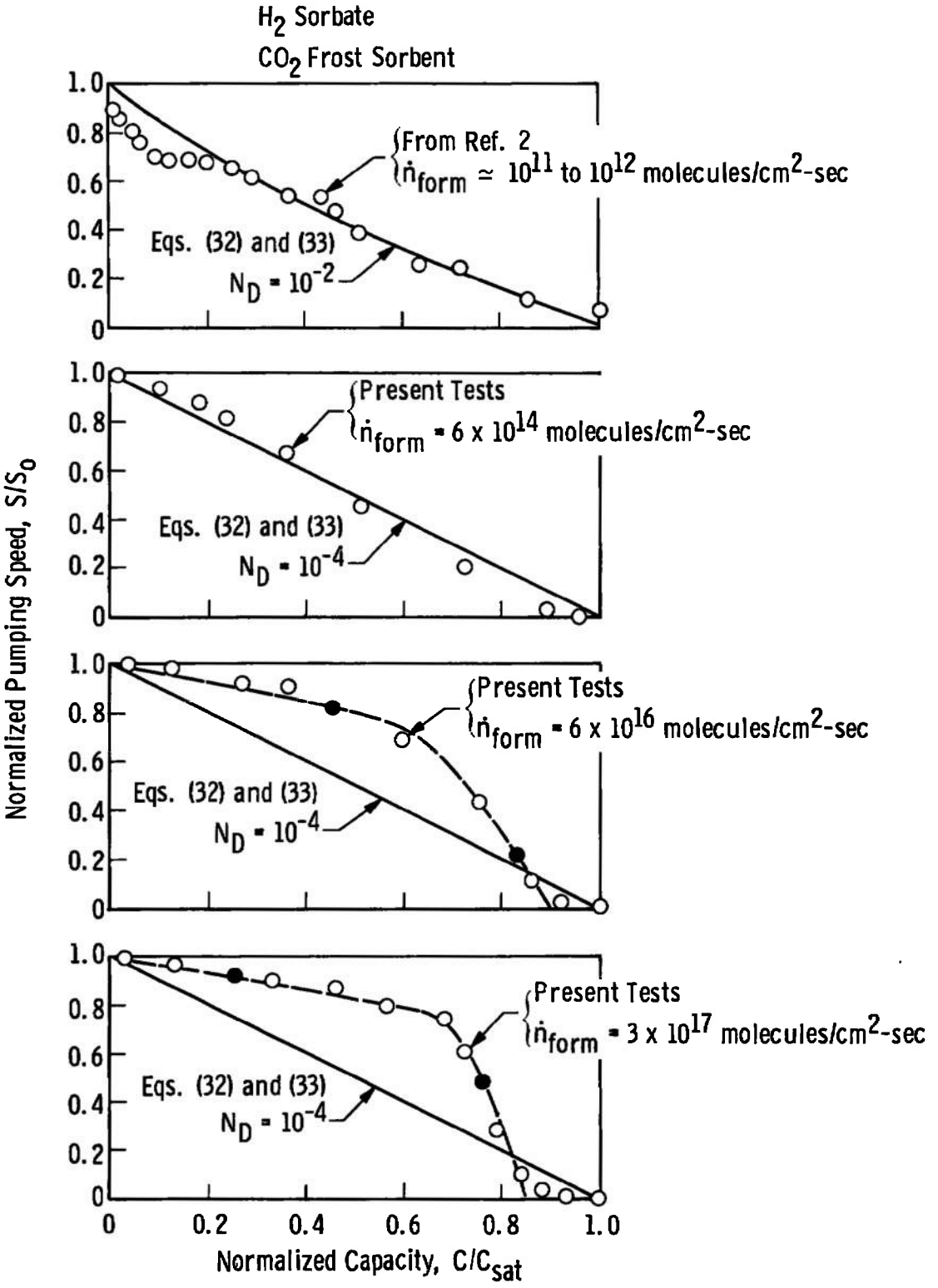

Fig. 20 Comparison of Theoretical Dynamic Sorption Pumping Curves with Experimental Results for Carbon Dioxide Sorbents of Different Porosities

APPENDIX II
DERIVATION OF EXPRESSIONS FOR PUMPING SPEED AND CAPACITY FOR THE TWO-LAYER MODEL

With the transformation

$$n' = n - n_o$$

the differential equations for this sorption pumping model become becomes

$$\frac{\partial n_1'(x,t)}{\partial t} = D_1 \frac{\partial^2 n_1'(x,t)}{\partial x^2} \tag{II-1}$$

$$\frac{\partial n_2'(x,t)}{\partial t} = D_2 \frac{\partial^2 n_2'(x,t)}{\partial x^2} \tag{II-2}$$

In addition, the boundary conditions are

$$n_1'(0,t) = n_2'(0,t) \tag{II-3}$$

$$D_1 \frac{\partial n_1'(0,t)}{\partial x} = D_2 \frac{\partial n_2'(0,t)}{\partial x} \tag{II-4}$$

$$n_1'(-\ell_1,t) = 0 \tag{II-5}$$

$$\frac{\partial n_2'(\ell_2,t)}{\partial x} = 0 \tag{II-6}$$

and the initial condition becomes

$$n_1'(x,0) = n_2'(x,0) = - n_o \tag{II-7}$$

Equations (II-1) and (II-2) may be solved by separation of variables assuming a product solution of the form

$$n' = T(t)X(x) \tag{II-8}$$

which has solutions

$$T(t) = C_1 e^{-\lambda^2 Dt} \tag{II-9}$$

and

$$X(x) = C_2 \cos \lambda x + C_3 \sin \lambda x \tag{II-10}$$

These individual solutions are combined to yield the general solution

$$n_1'(x,t) = e^{-\lambda_1^2 D_1 t} (A_1 \cos\lambda_1 x + B_1 \sin\lambda_1 x) \tag{II-11}$$

$$n_2'(x,t) = e^{-\lambda_2^2 D_2 t} (A_2 \cos\lambda_2 x + B_2 \sin\lambda_2 x) \tag{II-12}$$

Substituting Eqs. (II-11) and (II-12) into the boundary conditions [Eqs. (II-3) to (II-6)] leads to the following relationships between the constants:

$$B_1 = A_1 \cot(\lambda_1 \ell_1) \tag{II-13}$$

$$B_2 = A_2 \tan(\lambda_2 \ell_2) \tag{II-14}$$

$$A_1 = A_2 \frac{e^{-\lambda_2^2 D_2 t}}{e^{-\lambda_1^2 D_1 t}} \tag{II-15}$$

$$B_1 = B_2 \frac{(D_2\lambda_2) e^{-\lambda_2^2 D_2 t}}{(D_1\lambda_1) e^{-\lambda_1^2 D_1 t}} \tag{II-16}$$

which may be combined to obtain the characteristic equation

$$\cot(\lambda_1^{(n)} \ell_1) = \frac{D_2 \lambda_2^{(n)}}{D_1 \lambda_1^{(n)}} \tan(\lambda_2^{(n)} \ell_2) \tag{II-17}$$

The roots of Eq. (II-17) provide a set of characteristic values $\lambda_1^{(n)}$ and $\lambda_2^{(n)}$.

Because the equations are coupled at x = 0, the characteristic values, $\lambda_1^{(n)}$, are not independent of the values $\lambda_2^{(n)}$. This may be seen from Eqs. (II-15) and (II-16) which require that either

$$A_1 = A_2 = B_1 = B_2 \equiv 0 \tag{II-18}$$

or

$$\frac{d}{dt}\left[e^{-(\lambda_2^2 D_2 - \lambda_1^2 D_1)t}\right] \equiv 0 \tag{II-19}$$

The physical significance of Eq. (II-18) corresponds to the frost being saturated ($n = n_o$ = constant) which is the almost trival equilibrium case. Thus, in general, the second condition [Eq. (II-19)] must hold and

$$\lambda_1^2 D_1 = \lambda_2^2 D_2 \tag{II-20}$$

Then combining Eqs. (II-17) and (II-20) results in the characteristic equation

$$\cot\left[\sqrt{\frac{D_2}{D_1}}\ \lambda_2^{(n)} \ell_1\right] = \sqrt{\frac{D_2}{D_1}}\ \tan(\lambda_2^{(n)} \ell_2) \tag{II-21}$$

The roots of Eq. (II-21) yield one set of characteristic values, $\lambda_2^{(n)}$, although it could equivalently be written in terms of $\lambda_1^{(n)}$.

Inserting Eqs. (II-13) and (II-14) into Eqs. (II-11) and (II-12) and writing the result in terms of the characteristic values gives

$$n_1'(x,t) = A_1^{(n)}\ e^{-\lambda_1^{(n)2} D_1 t}\ (\cos[\lambda_1^{(n)} x + \cot(\lambda_1^{(n)} \ell_1)\ \sin\ \lambda_1^{(n)} x) \tag{II-22}$$

$$n_2'(x,t) = A_2^{(n)}\ e^{-\lambda_2^{(n)2} D_2 t}\ (\cos\ \lambda_2^{(n)} x + \tan(\lambda_2^{(n)} \ell_2)\ \sin\ \lambda_2^{(n)} x) \tag{II-23}$$

Since $(\lambda_1^{(n)})^2 D_1 = (\lambda_2^{(n)})^2 D_2$, it is seen from Eq. (II-15) that $A_1^{(n)} = A_2^{(n)}$. Using this fact and some simple trigonometric relationships and also assuming that the general solution can be written as a sum of the characteristic solutions allows Eqs. (II-22) and (II-23) to be rewritten as

$$n_1'(x,t) = \sum_{n=1}^{\infty} A_1^{(n)} \left[\frac{\sin\lambda_1^{(n)} (x+\ell_1)}{\sin[\lambda_1^{(n)} \ell_1]} \right] e^{-\lambda_1^{(n)2} D_1 t} \quad \text{(II-24)}$$

$$n_2'(x,t) = \sum_{n=1}^{\infty} A_1^{(n)} \left[\frac{\cos\lambda_2^{(n)} (x-\ell_2)}{\cos[\lambda_2^{(n)} \ell_2]} \right] e^{-\lambda_2^{(n)2} D_2 t} \quad \text{(II-25)}$$

The values of $A_1^{(n)}$ which correspond to the characteristic values of $\lambda_1^{(n)}$ and $\lambda_2^{(n)}$ may be obtained as Fourier coefficients by application of the initial condition [Eq. (II-7)], if the bracketed functions in Eqs. (II-24) and (II-25) are orthogonal.

When the initial condition is applied to Eqs. (II-24) and (II-25) and they become

$$- n_o = \sum_{n=1}^{\infty} A_1^{(n)} \psi^{(n)}(x) \quad \text{(II-26)}$$

where

$$\psi_1^{(n)}(x) = \frac{\sin\lambda_1^{(n)} (x+\ell_1)}{\sin\lambda_1^{(n)} \ell_1} \quad \text{for } -\ell_1 \le x \le 0 \quad \text{(II-27)}$$

$$\psi_2^{(n)}(x) = \frac{\cos\lambda_2^{(n)} (x-\ell_2)}{\cos\lambda_2^{(n)} \ell_2} \quad \text{for } 0 \le x \le \ell_2 \quad \text{(II-28)}$$

To determine the values of $A_1^{(n)}$, each region in Eqs. (II-27) and (II-28) may be multiplied by a corresponding function $\psi^{(m)}(x)$ and integrated over the intervals $-\ell_1$ to 0 and 0 to ℓ_2 for each region. Performing these operations on Eq. (II-26) results in

$$- n_o \int_{-\ell_1}^{0} \psi_1^{(m)}(x)dx - n_o \int_{0}^{\ell_2} \psi_2^{(m)}(x)dx =$$

$$= \sum_{n=1}^{\infty} A_1^{(n)} \left[\int_{-\ell_1}^{0} \psi_1^{(m)}(x)\ \psi_1^{(n)}(x)dx + \int_{0}^{\ell_2} \psi_2^{(m)}(x)\ \psi_2^{(n)}(x)dx \right] \tag{II-29}$$

If the functions $\psi^{(m)}(x)$ and $\psi^{(n)}(x)$ are orthogonal, then

$$\int \psi^{(m)}(x)\ \psi^{(n)}(x)dx = \begin{cases} \int \left[\psi_1^{(n)}(x)\right]^2 dx & m = n \\ 0 & m \neq n \end{cases}$$

and all of the integral terms in the summation on the right-hand side of Eq. (II-29) vanish except the term for m = n. Thus, Eq. (II-29) simplifies to

$$-n_o \int_{-\ell_1}^{0} \psi_1^{(n)}(x)dx - n_o \int_{0}^{\ell_2} \psi_2^{(n)}(x)dx$$

$$= A_1^{(n)} \left[\int_{-\ell_1}^{0} \left[\psi_1^{(n)}(x)\right]^2 dx + \int_{0}^{\ell_2} \left[\psi_2^{(n)}(x)\right]^2 dx \right] \tag{II-30}$$

Inserting Eqs. (II-27) and (II-28) into Eq. (II-30) and carrying out the integrations results in an expression for $A_1^{(n)}$:

$$-A_1^{(n)} = \left[\frac{2D_1 n_o}{\lambda_2^{(n)}}\right] \left[\frac{\sin\left(\lambda_2^{(n)}\ \ell_2\right) \cos\left(\lambda_2^{(n)}\ \ell_2\right) \cos\left(\lambda_1^{(n)}\ \ell_1\right)}{\ell_1 D_2 \sin^2\left(\lambda_2^{(n)}\ \ell_2\right) + D_1 \lambda_2 \cos^2\left(\lambda_1^{(n)}\ \ell_1\right)}\right] \tag{II-31}$$

It is yet necessary to prove that

$$\int_{-\ell_1}^{\ell_2} \psi^{(n)}(x)\ \psi^{(m)}(x)dx \equiv 0 \tag{II-32}$$

This may be rewritten for each region as

$$\Psi(x) = \int_{-\ell_1}^{\ell_2} \psi^{(n)}(x)\ \psi^{(m)}(x)dx$$

$$= \int_{-\ell_1}^{0} \frac{\sin[\lambda_1^{(n)}(x+\ell_1)]\ \sin[\lambda_1^{(m)}(x+\ell_1)]}{\sin(\lambda_1^{(n)}\ell_1)\ \sin(\lambda_1^{(m)}\ell_1)}\ dx$$

$$+ \int_{0}^{\ell_2} \frac{\cos[\lambda_2^{(n)}(x-\ell_2)]\ \cos[\lambda_2^{(m)}(x-\ell_2)]}{\cos(\lambda_2^{(n)}\ell_2)\ \cos(\lambda_2^{(m)}\ell_2)}\ dx \qquad \text{(II-33)}$$

Performing the integrations on the right-hand side results in

$$\Psi(x) = \frac{1}{\sin(\lambda_1^{(n)}\ell_1)\ \sin(\lambda_1^{(m)}\ell_1)}\left[\frac{\sin([\lambda_1^{(n)} - \lambda_1^{(m)}]\ell_1)}{2(\lambda_1^{(n)} - \lambda_1^{(m)})}\right.$$

$$\left. - \frac{\sin([\lambda_1^{(n)} + \lambda_1^{(m)}]\ell_1)}{2(\lambda_1^{(n)} + \lambda_1^{(m)})}\right] + \frac{1}{\cos(\lambda_2^{(n)}\ell_2)\ \cos(\lambda_2^{(m)}\ell_2)}$$

$$\times \left[\frac{\sin([\lambda_2^{(n)} - \lambda_2^{(m)}]\ell_2)}{2(\lambda_2^{(n)} - \lambda_2^{(m)})} + \frac{\sin([\lambda_2^{(n)} + \lambda_2^{(m)}]\ell_2)}{2(\lambda_2^{(n)} + \lambda_2^{(m)})}\right] \qquad \text{(II-34)}$$

Recalling Eqs. (II-17) and (II-20),

$$\cot(\lambda_1^{(n)}\ \ell_1) = \frac{D_2\lambda_2^{(n)}}{D_1\lambda_1^{(n)}} \tan(\lambda_2^{(n)}\ \ell_2)$$

$$\lambda_1^{\ 2} D_1 = \lambda_2^{\ 2} D_2$$

which may be combined to give

$$\tan(\lambda_2\ell_2) = \frac{\lambda_2}{\lambda_1} \cot(\lambda_1\ell_1) \tag{II-35}$$

and, using formulae for the trigonometric functions of the sums and differences of angles, allows Eq. (II-34) to be rewritten and simplified to

$$\Psi(x) = \left[\frac{1}{\lambda_1^{(n)} - \lambda_1^{(m)}} - \frac{\lambda_2^{(m)}/\lambda_1^{(m)}}{\lambda_2^{(n)} - \lambda_2^{(m)}} + \frac{\lambda_2^{(m)}/\lambda_1^{(m)}}{\lambda_2^{(n)} + \lambda_2^{(m)}}\right.$$

$$\left. - \frac{1}{\lambda_1^{(n)} + \lambda_1^{(m)}}\right] \frac{\cot[\lambda_1^{(m)}\ell_1]}{2} + \left[\frac{\lambda_2^{(n)}/\lambda_1^{(n)}}{\lambda_2^{(n)} - \lambda_2^{(m)}}\right.$$

$$\left. - \frac{1}{\lambda_1^{(n)} - \lambda_1^{(m)}} + \frac{\lambda_2^{(n)}/\lambda_1^{(n)}}{\lambda_2^{(n)} + \lambda_2^{(m)}} - \frac{1}{\lambda_1^{(n)} + \lambda_1^{(m)}}\right] \frac{\cot\lambda_1^{(n)}\ell_1}{2} \tag{II-36}$$

Now, if the bracketed terms of Eq. (II-36) are equal to zero, then $\Psi(x) = 0$. When the first of these [i.e., the coefficient of cot $(\lambda_1{}^{(m)}\ell_1)$] is rewritten with a common denominator, expanded and simplified, there results

$$\left[\frac{[\lambda_1^{(m)}]^2\,[\lambda_2^{(n)}]^2 - [\lambda_1^{(n)}]^2\,[\lambda_2^{(m)}]^2}{[\lambda_1^{(n)} - \lambda_1^{(m)}]\,[\lambda_2^{(n)} - \lambda_2^{(m)}]\,[\lambda_2^{(n)} + \lambda_2^{(m)}]\,[\lambda_1^{(n)} + \lambda_2^{(m)}]}\right]\frac{2}{\lambda_1^{(m)}} \tag{II-37}$$

From Eq. (II-20), one may write

$$[\lambda_1^{(n)}]^2 D_1 = [\lambda_2^{(n)}]^2 D_2$$

and (II-38)

$$[\lambda_1^{(m)}]^2 D_1 = [\lambda_2^{(m)}]^2 D_2$$

When Eqs. (II-38) are inserted into Eq. (II-37), the numerator vanishes; consequently, the coefficient of cot $(\lambda_1^{(m)}\ell_1)$ in Eq. (II-36) is zero. Similarly, it may be shown that the second bracketed term of Eq. (II-36) vanishes. Hence, this means

$$\int_{-\ell_1}^{\ell_2} \psi^{(n)}(x)\,\psi^{(m)}(x)\,dx = 0$$

and $\Psi^{(n)}(x)$ and $\Psi^{(m)}(x)$ are orthogonal. Thus, Eq. (II-31) provides a set of Fourier coefficients which when inserted in Eqs. (II-24) and (II-25) result in a set of equations giving the number densities of sorbed molecules in the frost as a function of x and t. The eigenvalues for these equations are specified by Eq. (II-21).

TABLE I
CONSTANTS IN LENNARD-JONES 6-12 POTENTIAL

Gas	σ	ϵ_k/k	$\epsilon_k - H_2/k$
H_2	2.915	38.0	38.0
Ar	3.465	116.0	66.3
Xe	4.055	229.0	93.2
N_2	3.749	79.8	55.2
O_2	3.541	88.0	61.4
CO_2	3.897	213.0	79.5
N_2O	3.816	237.0	85.6
SF_6			89.1
CCl_4	5.881	327.0	111.0
Cl_2	4.115	357.0	115.5
Hg	2.898	851.0	179.0
$SnCl_4$	4.540	1550.0	242.0
C_6H_6	5.270	440.0	129.0
nC_8H_{18}	7.450	320.0	110.0
CH_3OH	3.858	507.0	138.0
CH_3Cl	3.375	855.0	179.0
COS	4.130	335.0	112.0
H_2O	2.650	380	121.0
CS_2	4.438	488.0	135.0

TABLE II
VALUES OF n_o AND D_1/ℓ_1 FOR HYDROGEN SORBED BY VARIOUS FROSTS

Sorbent	P_{form}, torr	T_f, °K	ℓ_f, cm	V_f, cm^3	C_{sat}	n_o, molecules/cm^3	s_o, liters/sec-cm^2	J_o, molecules/sec-$cm^2 \times 10^{-13}$	(D_1/ℓ_1) cm/sec $\times 10^8$	Source
CO_2	10^{-9} to 10^{-8}	11	2.7×10^{-6}	0.015	0.050	9.5×10^{20}	23.2	7.6	8.0	Ref. 2
Ar	↓	↓	2.5×10^{-6}	0.019	0.015	6.5×10^{20}	4.7	1.6	2.5	↓
N_2			5.7×10^{-6}	0.030	0.013	2.5×10^{20}	3.2	1.1	4.4	
O_2			2.8×10^{-6}	0.015	0.014	5.0×10^{20}	7.3	2.5	5.0	
H_2O			2.7×10^{-6}	0.014	0.040	8.0×10^{20}	44.9	15.2	1.9	
CO_2	2×10^{-6}	12.4	1×10^{-4}	0.097	0.26	5.6×10^{21}	31.0	9.3	1.6	Present Study
	2×10^{-5}	↓	↓	↓	0.35	7.5×10^{21}	31.0	9.3	1.2	↓
	2×10^{-4}				0.45	9.6×10^{21}	29.0	8.7	0.9	
	1×10^{-3}				0.48	1.0×10^{22}	27.0	8.1	0.8	
CO_2	2×10^{-5}	12.4	1×10^{-4}	0.097	0.35	7.5×10^{21}	31.0	9.3	1.2	↓
	↓	16.5	↓	0.097	0.18	3.8×10^{21}	25.0	7.2	1.9	
		21.5		↓	0.04	0.8×10^{21}	20.0	6.0	7.5	

TABLE III
APPARENT DIFFUSION CONSTANTS FOR HYDROGEN IN VARIOUS FROST SPECIES

Frost Species	P_{form}, torr	T_f, °K	D_2, cm^2/sec	σ, Å
CO_2	10^{-9} to 10^{-8}	11	2.0×10^{-11}	3.897
N_2	↓	↓	2.5×10^{-13}	3.749
O_2	↓	↓	1.6×10^{-14}	3.541
Ar	↓	↓	1.6×10^{-14}	3.465
H_2O	↓	↓	1.0×10^{-15}	2.650

UNCLASSIFIED

Security Classification

DOCUMENT CONTROL DATA - R & D

(Security classification of title, body of abstract and indexing annotation must be entered when the overall report is classified)

1. ORIGINATING ACTIVITY (Corporate author)	2a. REPORT SECURITY CLASSIFICATION
Arnold Engineering Development Center ARO, Inc., Operating Contractor Arnold Air Force Station, Tennessee	UNCLASSIFIED
	2b. GROUP N/A

3. REPORT TITLE

SORPTION PUMPING OF HYDROGEN BY CRYODEPOSITS--DYNAMIC PUMPING CHARACTERISTICS

4 DESCRIPTIVE NOTES (Type of report and inclusive dates)

Final Report - April 1969 through September 1969

5. AUTHOR(S) (First name, middle initial, last name)

K. E. Tempelmeyer, ARO, Inc.

6. REPORT DATE	7a. TOTAL NO. OF PAGES	7b. NO. OF REFS
October 1970	74	31

8a. CONTRACT OR GRANT NO	9a. ORIGINATOR'S REPORT NUMBER(S)
F40600-71-C-0002	
b. PROJECT NO.	AEDC-TR-70-102
c. Program Element 61120F	9b. OTHER REPORT NO(S) (Any other numbers that may be assigned this report)
d.	ARO-VKF-TR-70-102

10. DISTRIBUTION STATEMENT

This document has been approved for public release and sale; its distribution is unlimited.

11 SUPPLEMENTARY NOTES	12. SPONSORING MILITARY ACTIVITY
Available in DDC	Arnold Engineering Development Center Air Force Systems Command Arnold Air Force Station, Tennessee 37389

13 ABSTRACT The sorption for cryodeposited frosts for hydrogen has been investigated both analytically and experimentally. Most of the experimental tests were carried out with carbon dioxide frost at temperatures between 12 and 22°K as the cryosorbent and hydrogen at 300°K as the sorbate. Dynamic pumping characteristics of the sorbent-sorbate combination were systematically measured for chamber pressures between 10^{-7} and 10^{-4} torr. Additional experimental results were obtained with sulphur dioxide and methyl chloride cryosorbents. An initial hydrogen pumping speed of 30 liters/cm^2-sec was measured for 12°K carbon dioxide frost which was equivalent to an initial effective capture probability of about 0.7. The initial pumping speed appears to be governed by the sorbent, sorbate-surface interaction and may be increased somewhat by forming the surface in a manner to make it smoother but at the consequence of an attendant loss of sorption capacity. The pumping speed of a frost cryosorbent decreases with increasing amount of gas sorbed. A model of the sorption dynamics was formulated. An approximate closed-form solution was obtained in the limit of rather compact frosts whose sorption behavior would be limited by ability of the molecules to penetrate and diffuse into the frost. Theoretical calculations for this limiting case agreed with the observed pumping characteristics of the more compact frosts. Consequently, it is believed that the formulation of the frost cryosorption theory is proper. Comparisons between theory and experiment indicated that the diffusion constant for hydrogen in a variety of cryodeposits varied from 10^{-8} to 10^{-15} cm^2/sec. Also, it was noted that carbon dioxide and sulphur dioxide frosts deposited at temperatures below 30°K appear to undergo some crystal transition if their temperature is increased to above 30°K.

DD FORM 1 NOV 65 1473

UNCLASSIFIED

Security Classification

14. KEY WORDS	LINK A		LINK B		LINK C	
	ROLE	WT	ROLE	WT	ROLE	WT
1 cryogenics						
3 cryosorption						
2 cryopumping						
4 hydrogen -- Pumping						
5 carbon dioxide						
6 vacuum pumps						
7 sorption						

AFSC
Arnold AFS Tenn